Chapter 3. 銀河形成理論

宇宙背景輻射の測定の歴史

1965 Penzias and Wilson

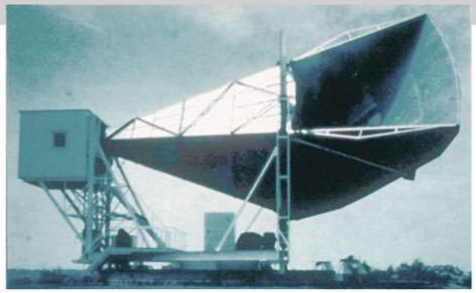

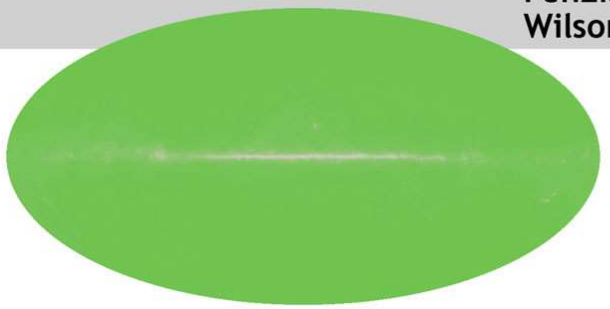

1992 COBE

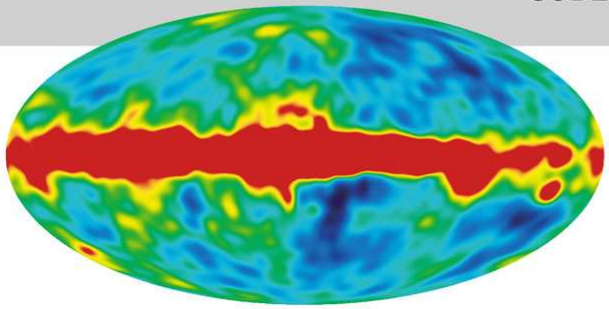

2003 WMAP

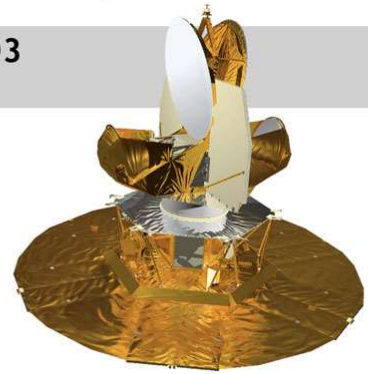

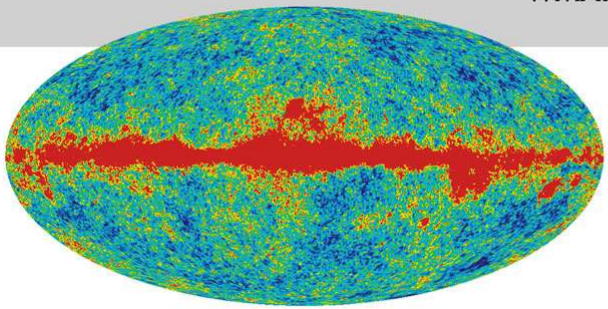

Wilkinson Microwave Anisotropy Probe (WMAP)
宇宙背景輻射の温度パターン

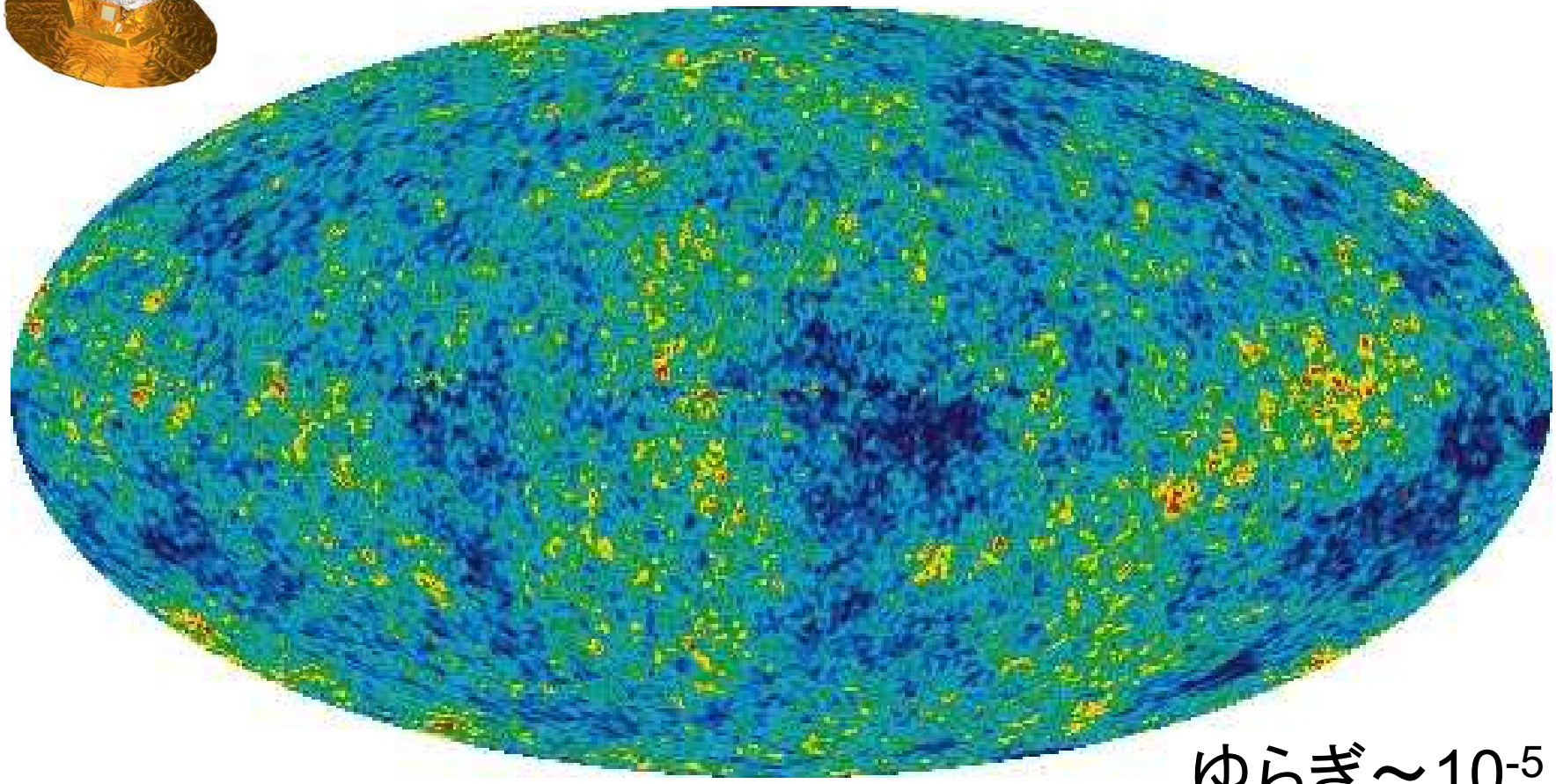

ゆらぎ～10^{-5}

揺らぎの時間発展

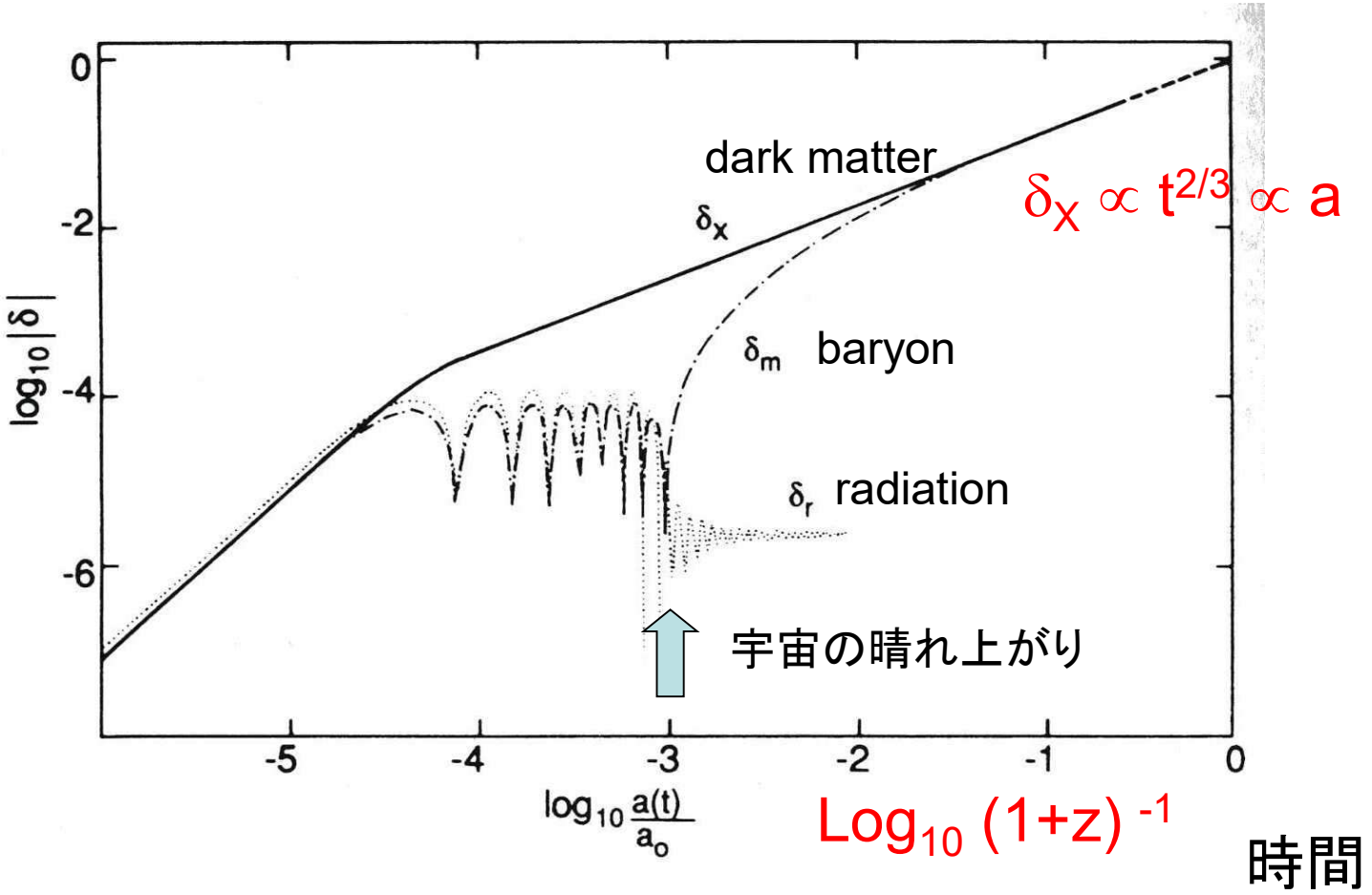

Figure 13.3 Evolution of perturbations on a scale $M \simeq 10^{15}\ \mathrm{M}_\odot$ for the cold component δ_X, baryonic component δ_m and photons δ_r in a model dominated by CDM ($\Omega = 1$, $h = 0.5$).

密度ゆらぎのパワースペクトラム

log $|k^{3/2}\delta_k|$

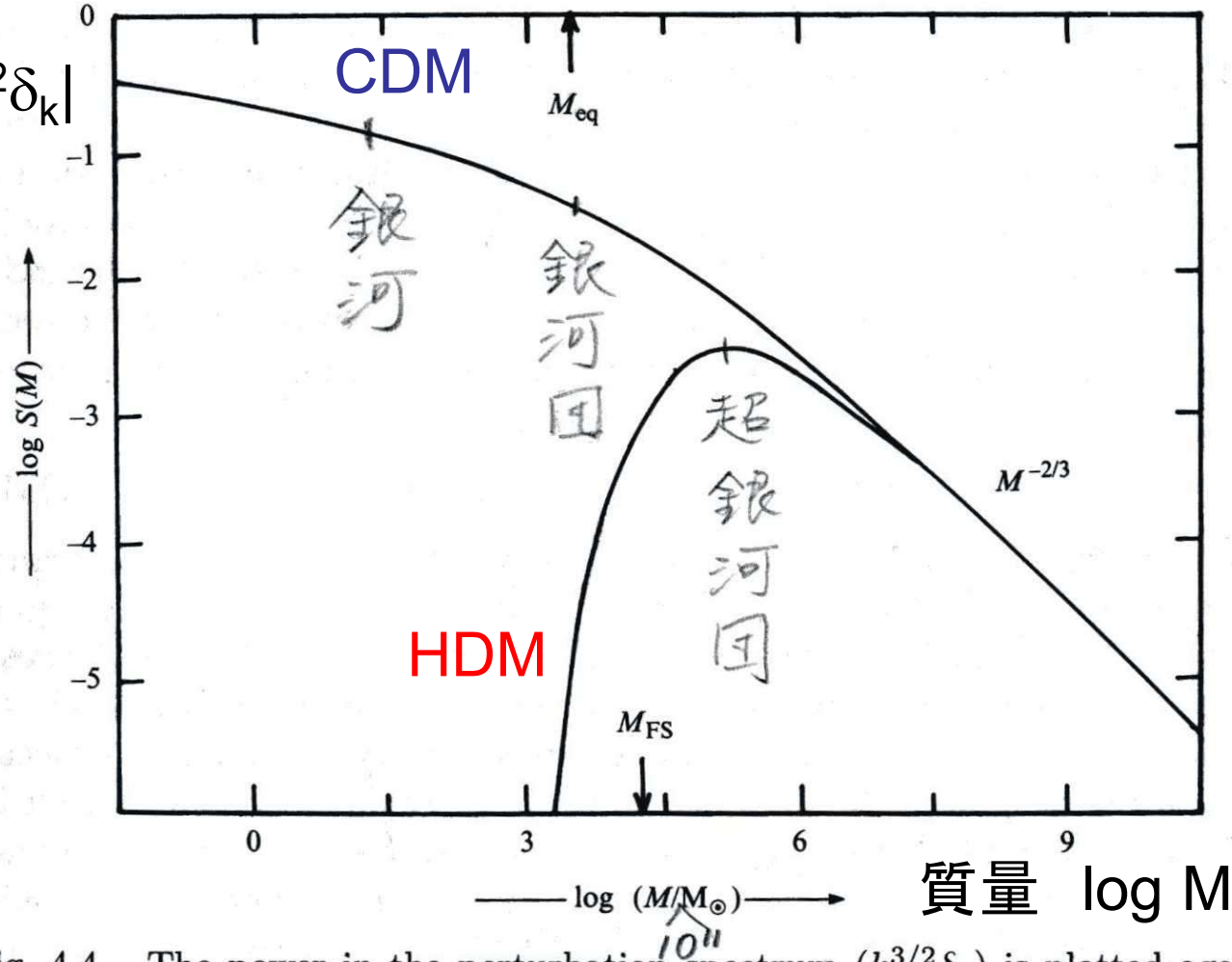

質量 log $M/10^{11}M_{sun}$

Fig. 4.4. The power in the perturbation spectrum ($k^{3/2}\delta_k$) is plotted against the mass contained in the perturbation. The initial spectrum is assumed to be scale invariant. In scenarios with hot dark matter, the spectrum is peaked at M_{FS}, while in scenarios with cold dark matter, there is a relatively flat, gently sloping-down portion, between M_{FS} and M_{eq}. The power falls as $M^{-2/3}$ at large scales.

CDM

HDM

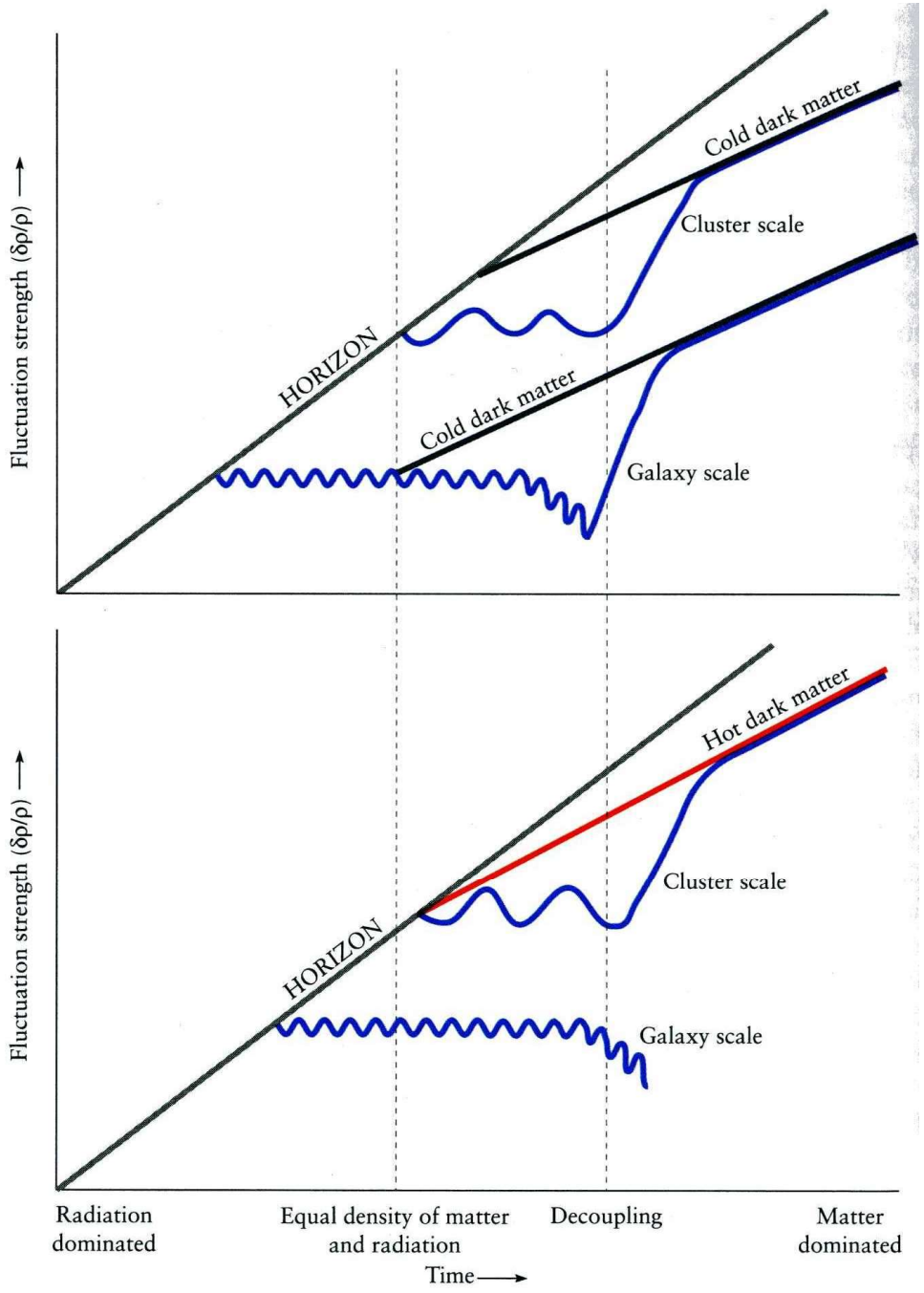
Fluctuation strength (δρ/ρ) ⟶
Cold dark matter
Cluster scale
HORIZON
Cold dark matter
Galaxy scale
Fluctuation strength (δρ/ρ) ⟶
Hot dark matter
Cluster scale
HORIZON
Galaxy scale
Radiation dominated
Equal density of matter and radiation
Decoupling
Matter dominated
Time ⟶

時間

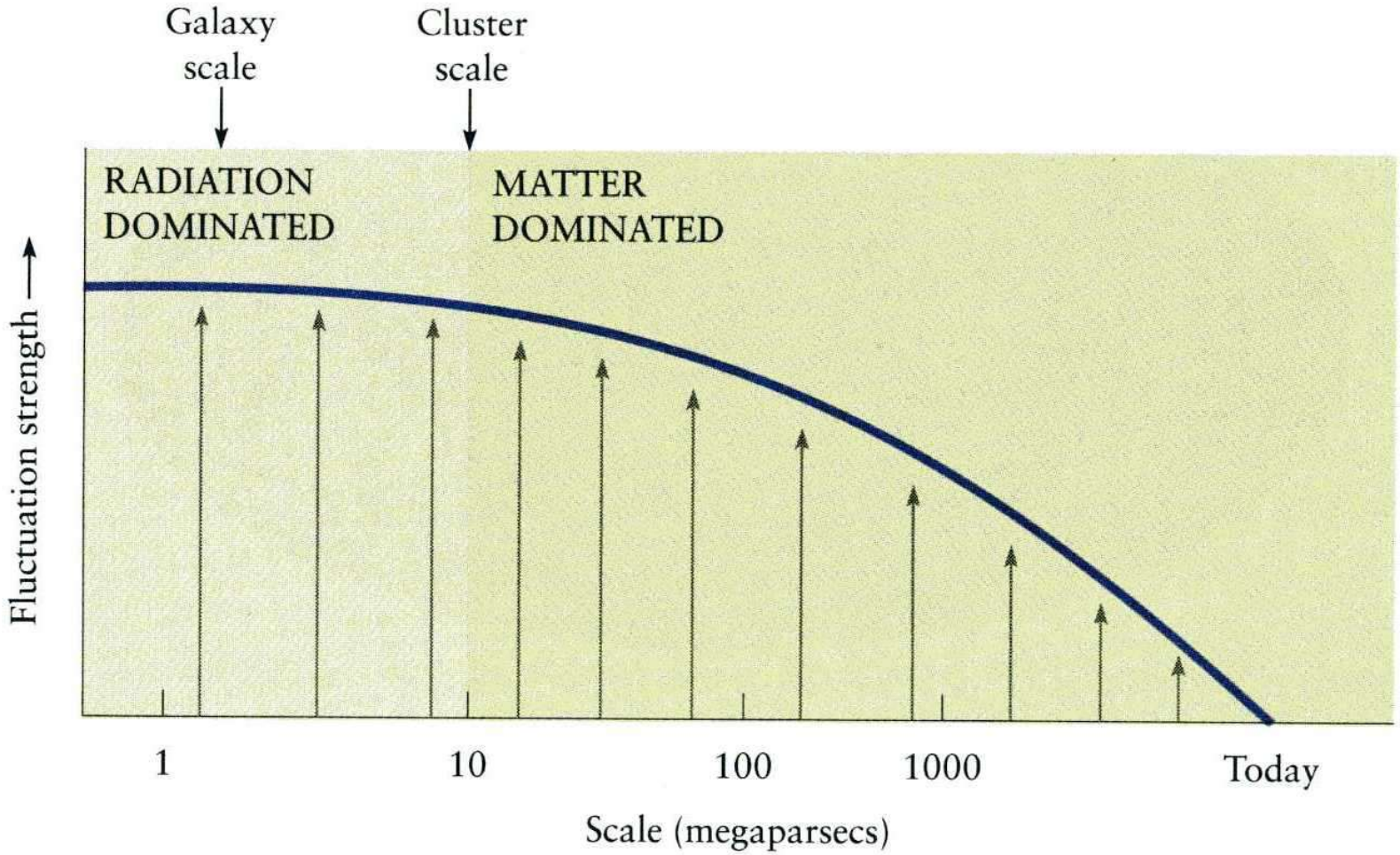
Galaxy scale
Cluster scale
RADIATION DOMINATED
MATTER DOMINATED
Fluctuation strength
1
10
100
1000
Today
Scale (megaparsecs)

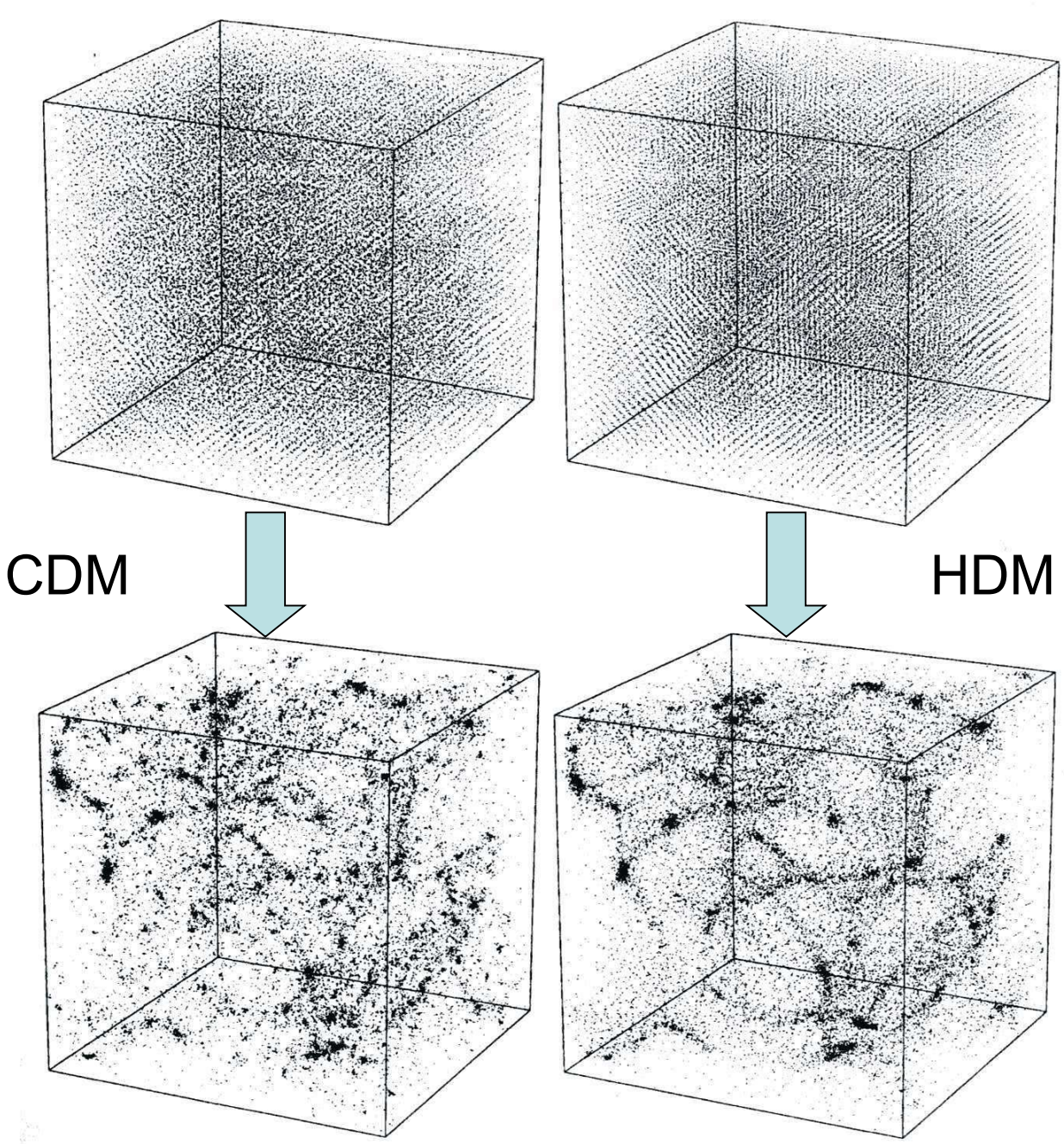
CDM
HDM

galaxy distributions in the sky

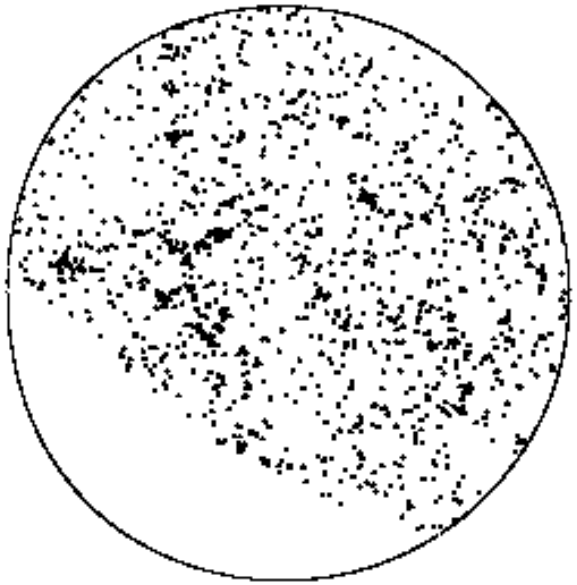

Cold dark matter

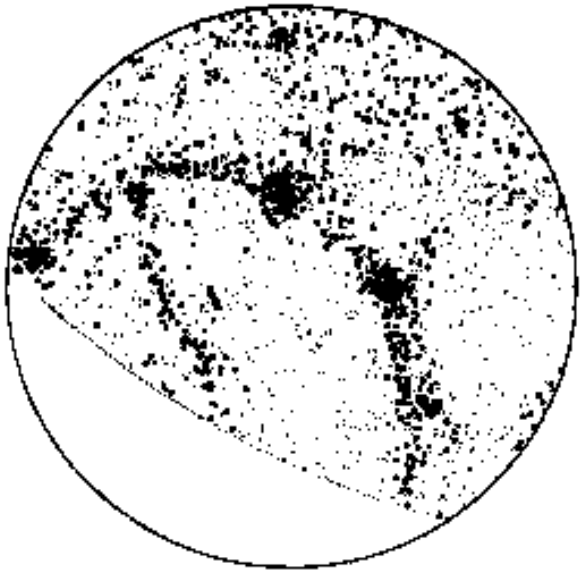

Hot dark matter

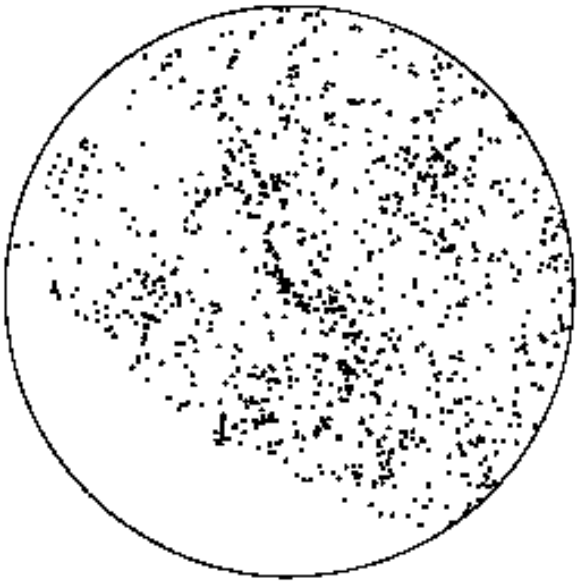

Actual data

- Hot Dark Matter (HDM) e.g. neutrino
  - ✓ free streaming suppresses small-scale fluctuations
- Cold Dark Matter (CDM) e.g. neutralino
  - ✓ smaller scales form earlier

宇宙の大規模構造のスケール依存性

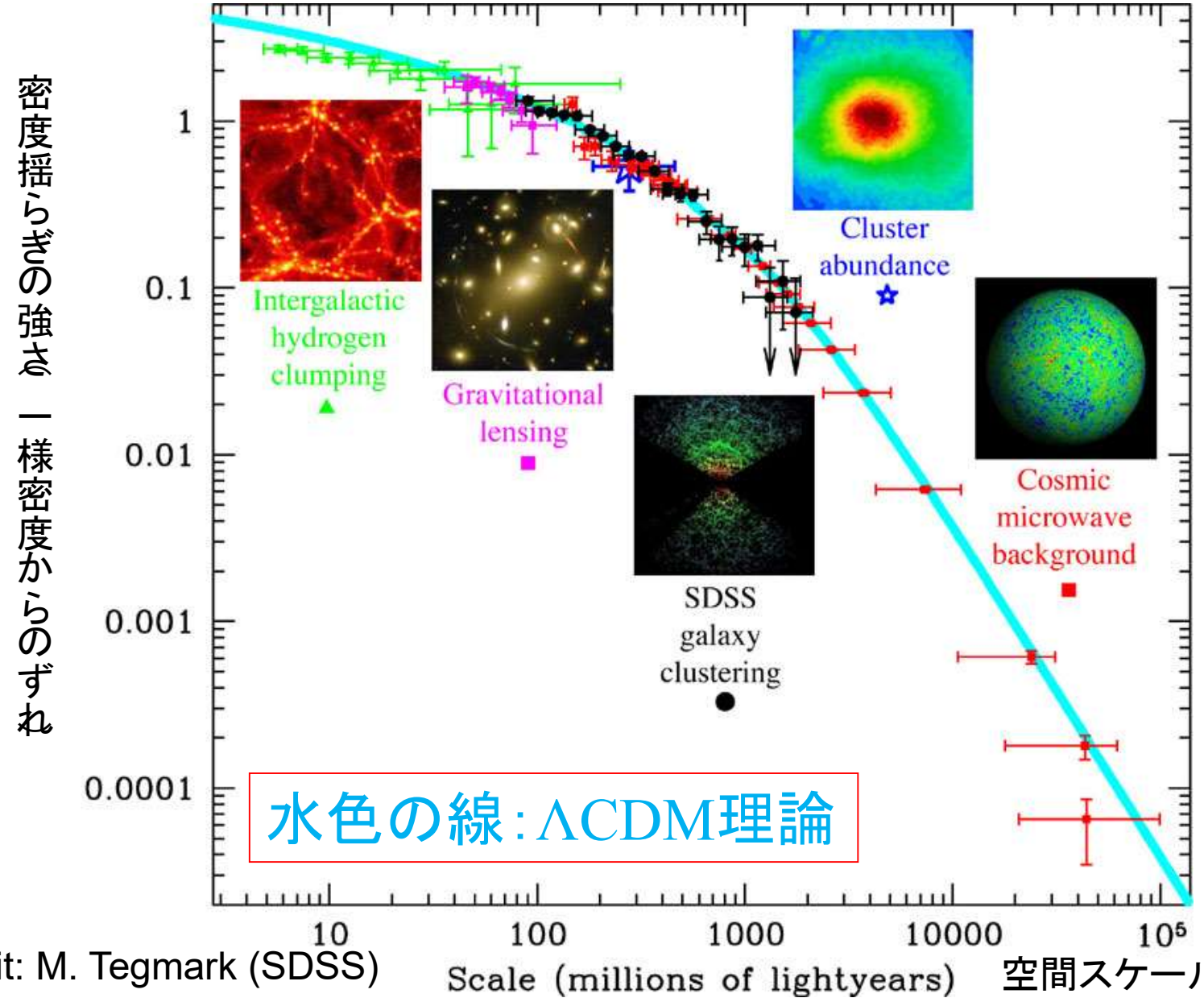

Credit: M. Tegmark (SDSS)

宇宙の平均密度と密度揺らぎの時間発展

ρ

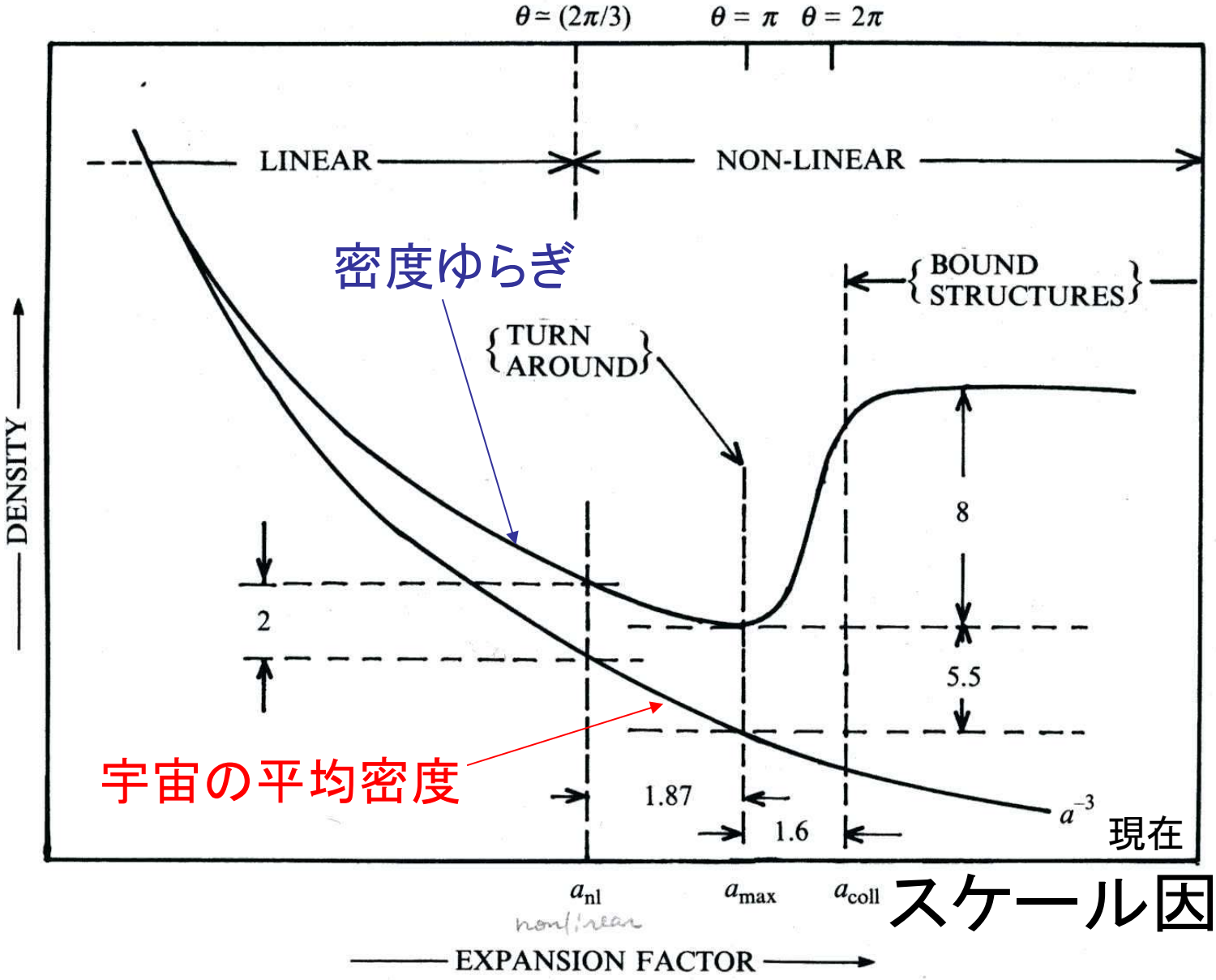

スケール因子a

原始（ゼロメタル）ガスの冷却関数

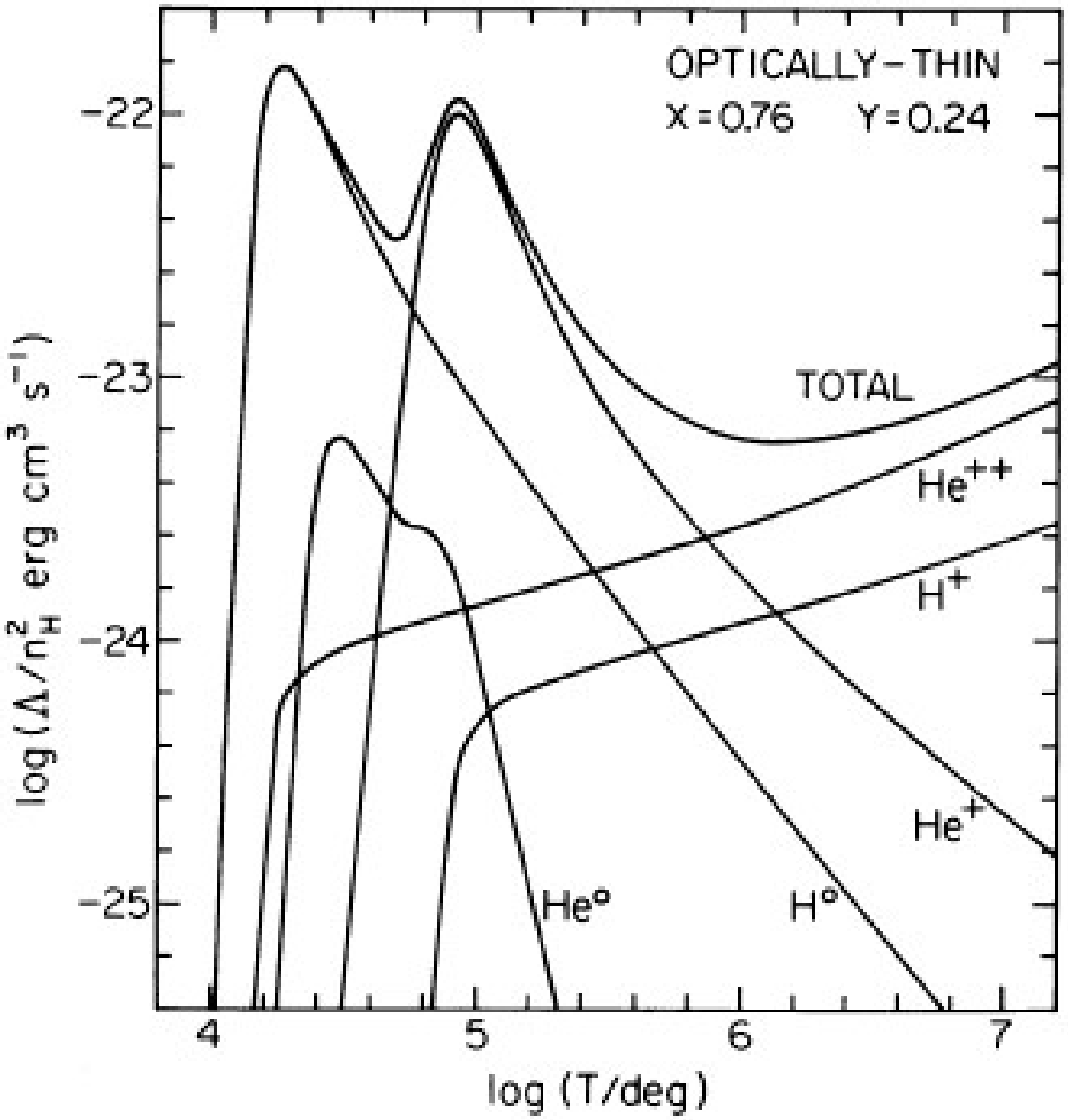

Fall & Rees 1985

金属量が有限なガスの冷却関数

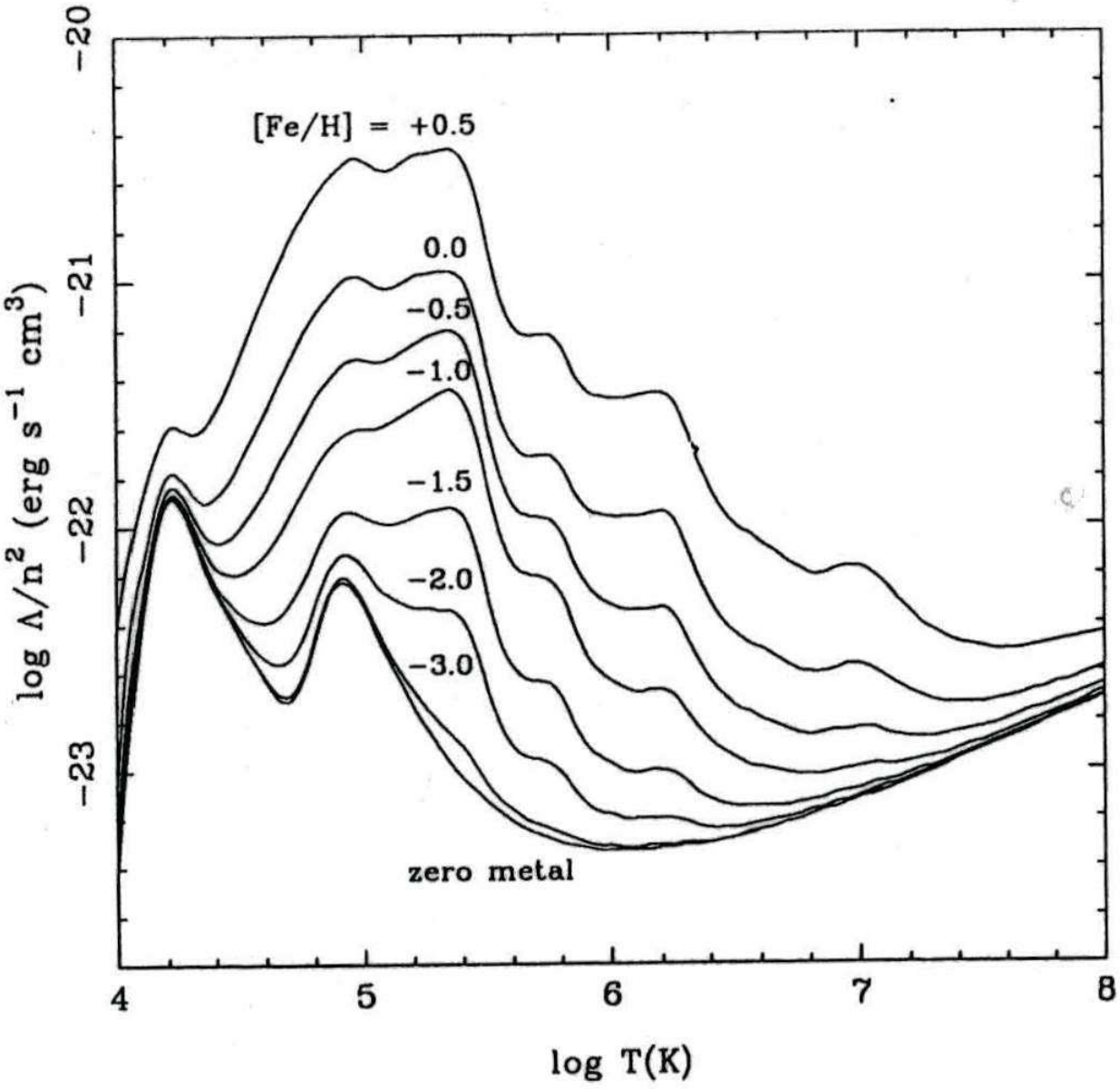

Cooling diagram

Rees & Ostriker 1977

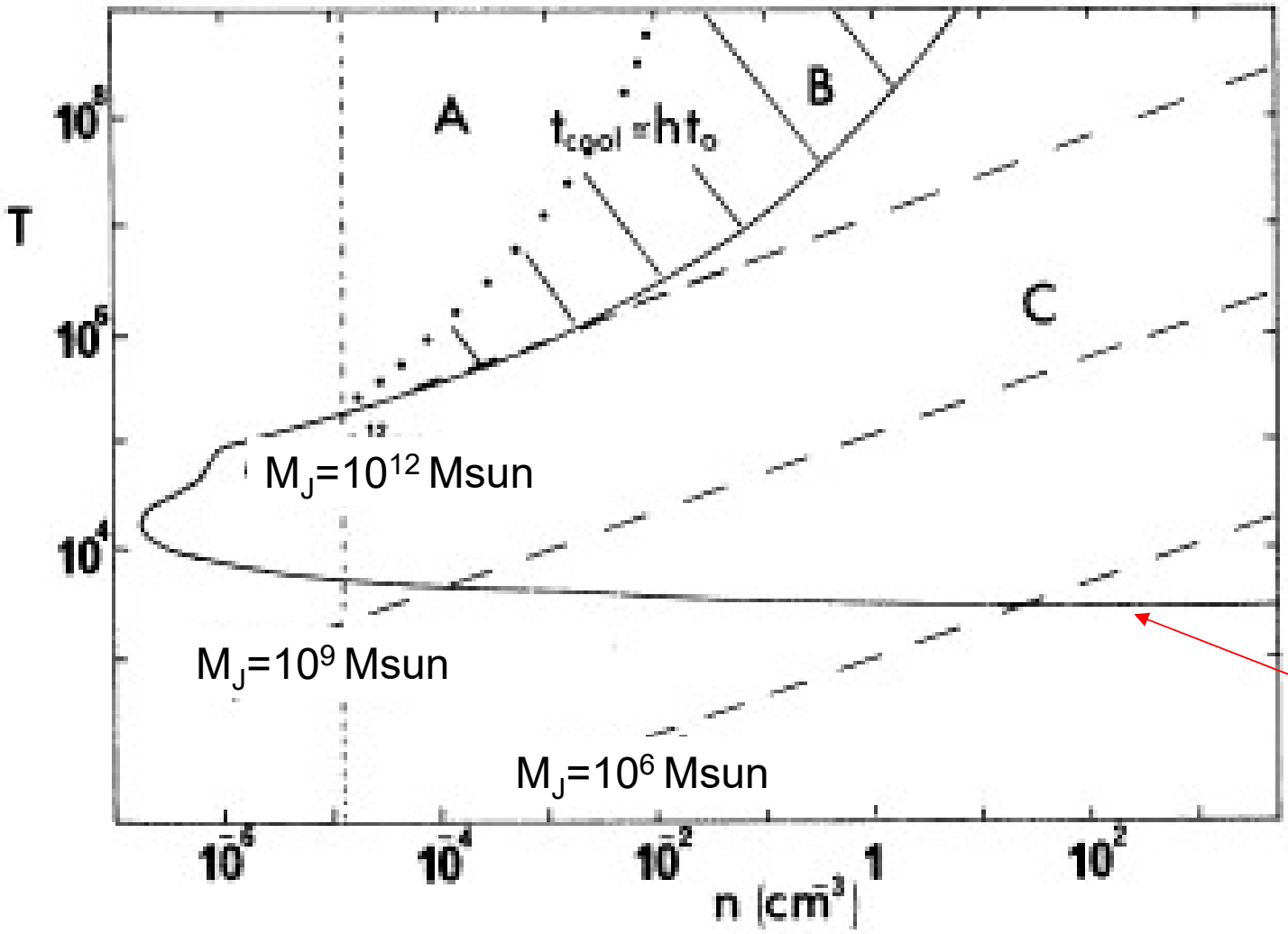

A: $t_{cool}>t_0$

B: $t_0>t_{cool}>t_{ff}$

C: $t_{cool}<t_{ff}$

$\tau = 1$

Rees & Ostriker 1977

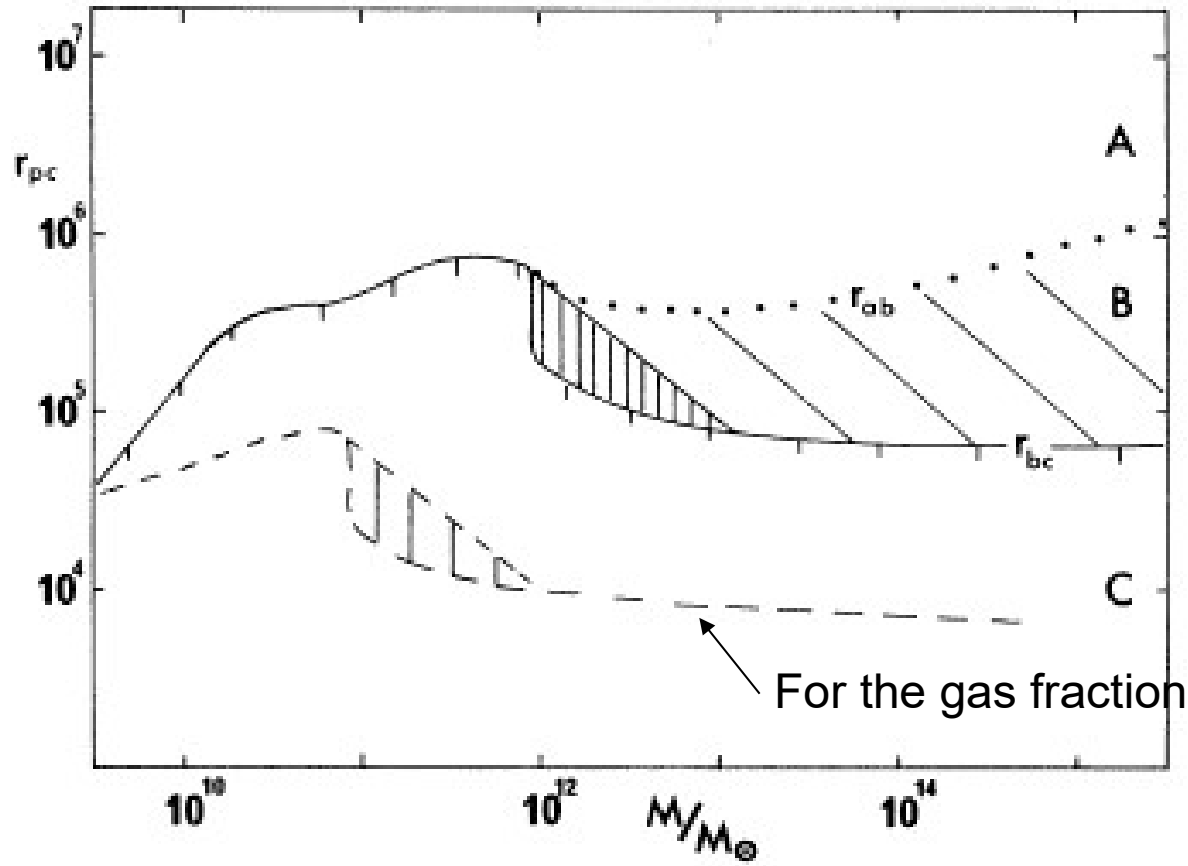

(pc)

~ 75kpc

For the gas fraction of 0.9

Figure 2. Information essentially similar to that in Fig. 1 is here plotted in terms of cloud mass and cloud radius. The mass-dependent radii demarcating domains A, B and C are denoted by r_{ab} and r_{bc}. Note that at large masses r_{bc} has a constant value $\simeq 75$ kpc. When a fraction x of the cloud has been converted into stars, the remaining gas can be quasistatically supported down to a smaller radius, obtained by shifting the previous curve downwards and to the left by a factor $(1-x)^{-1}$. The dashed curve corresponds to the case $x = 0.9$. When T_{virial} is in the range of temperatures where $\Lambda(T)$ decreases with T, a cloud can in fact radiate *more* energy at a *lower* temperature. This could increase r_{bc} for masses 10^{11}–$10^{13}\,M_\odot$ to an extent that is indicated by the region of vertical shading.

Cooling diagram

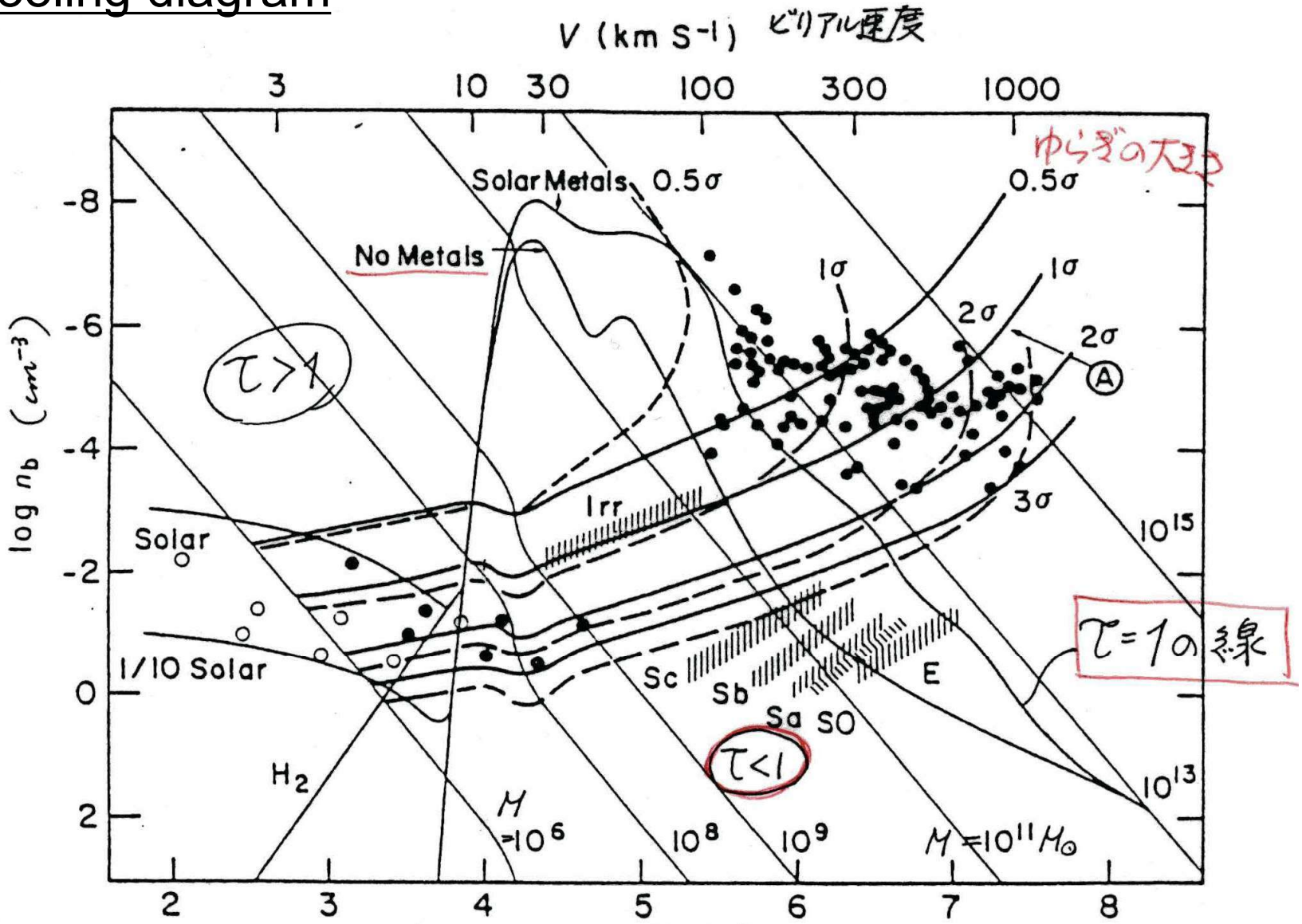

バリオンの数密度

温度

Blumenthal, Faber, Primack, & Rees 1984

冷たいガス流（cold stream）による銀河形成
Dekel et al. (2009)

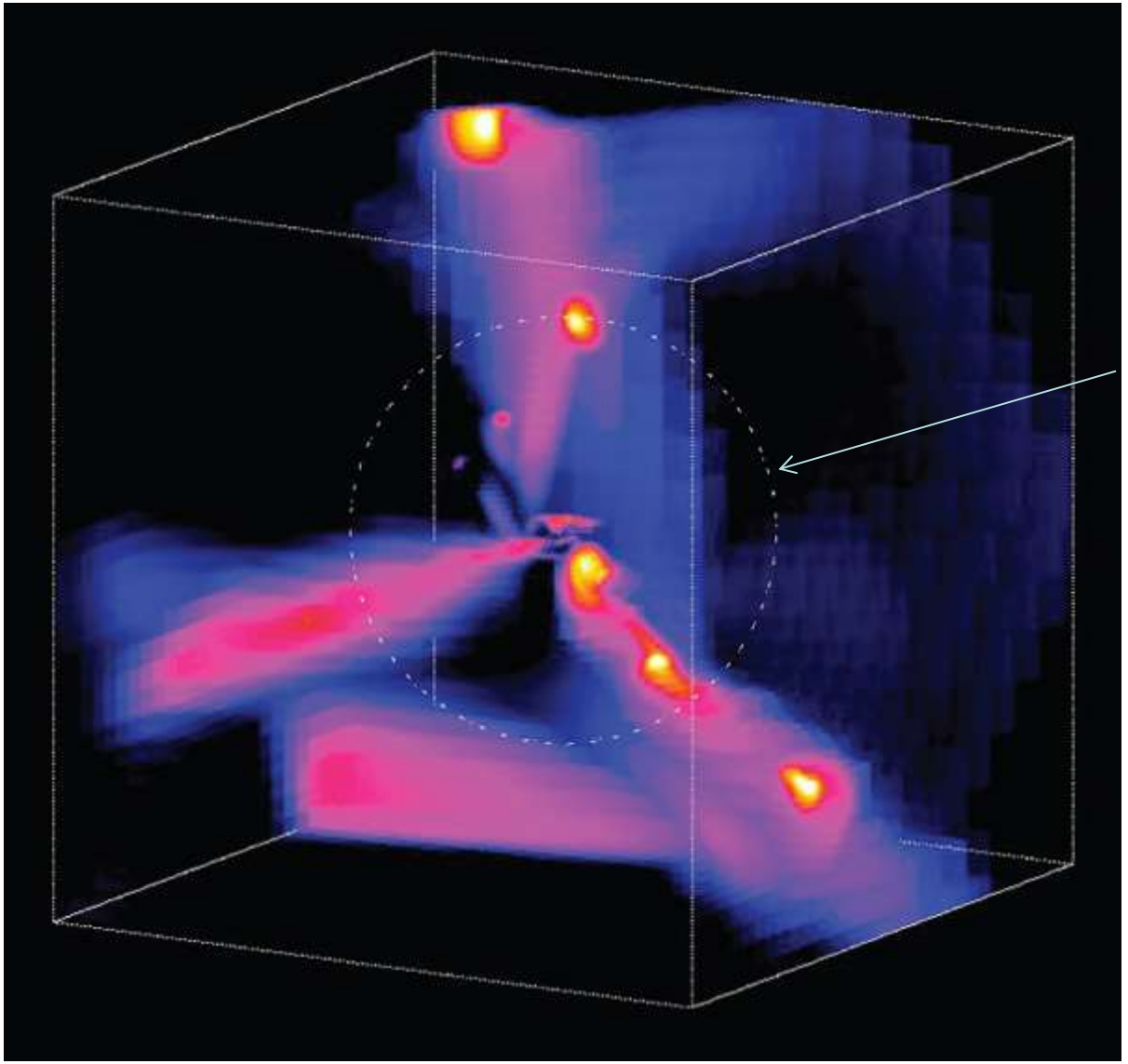

Cold flows or shock heating

Hot mode
(shock heating)

Cold mode
(streams)

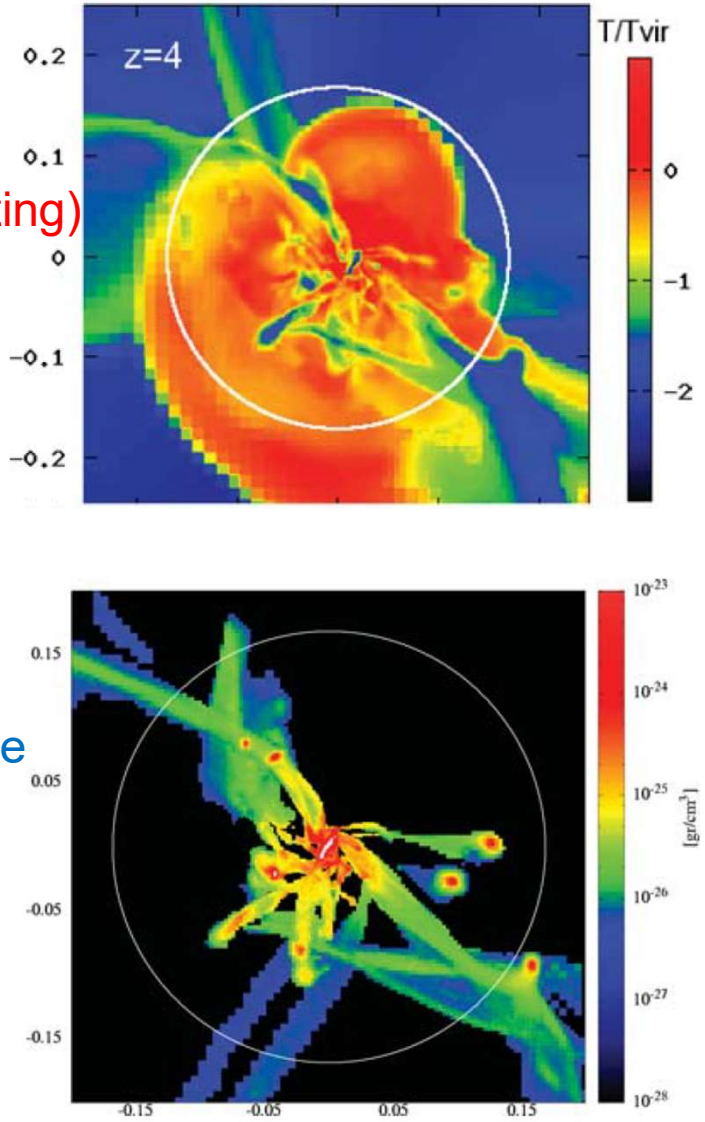

Dekel & Birnboim 2006

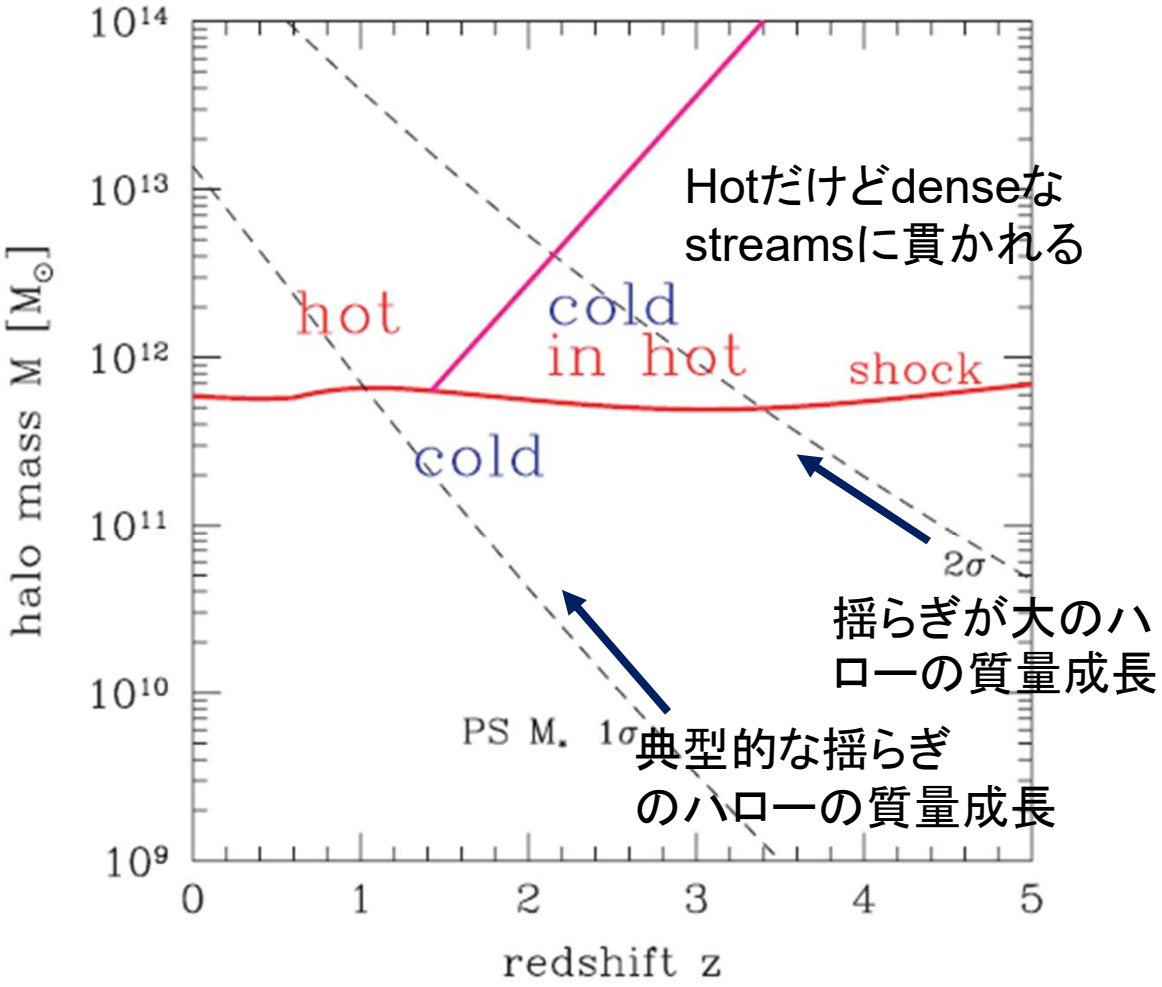

Figure 7. Cold streams and shock-heated medium as a function of halo mass and redshift. The nearly horizontal curve is the typical threshold mass for a

高赤方偏移銀河の回転運動

z=2.38にある若い円盤銀河のHα線観測　Genzel et al. (2006)

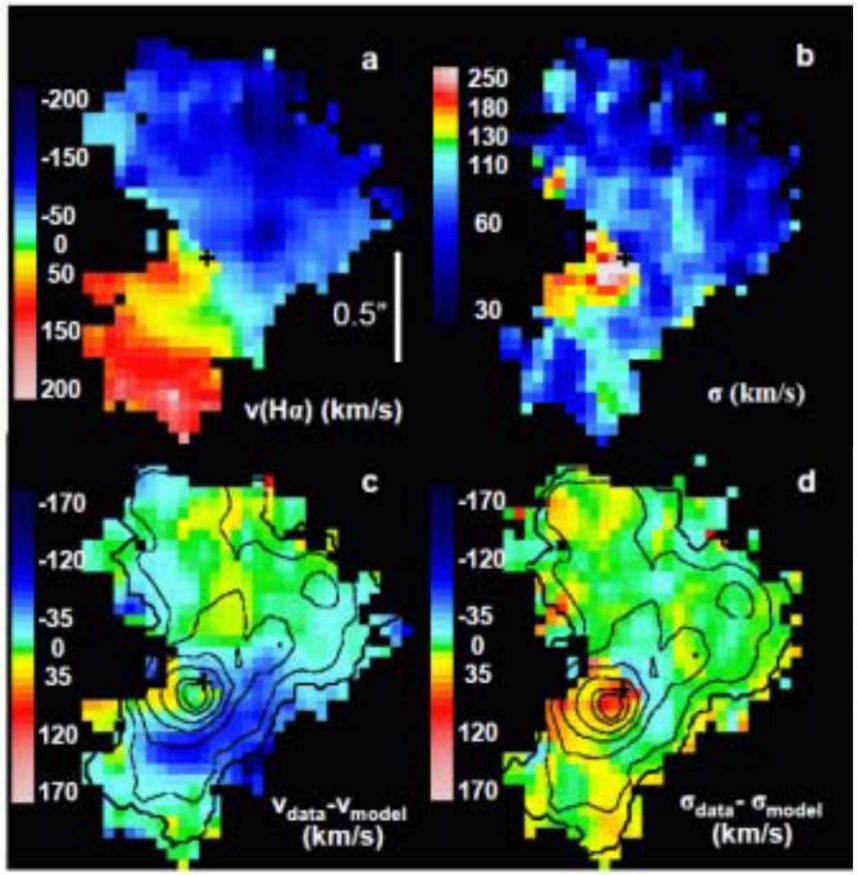

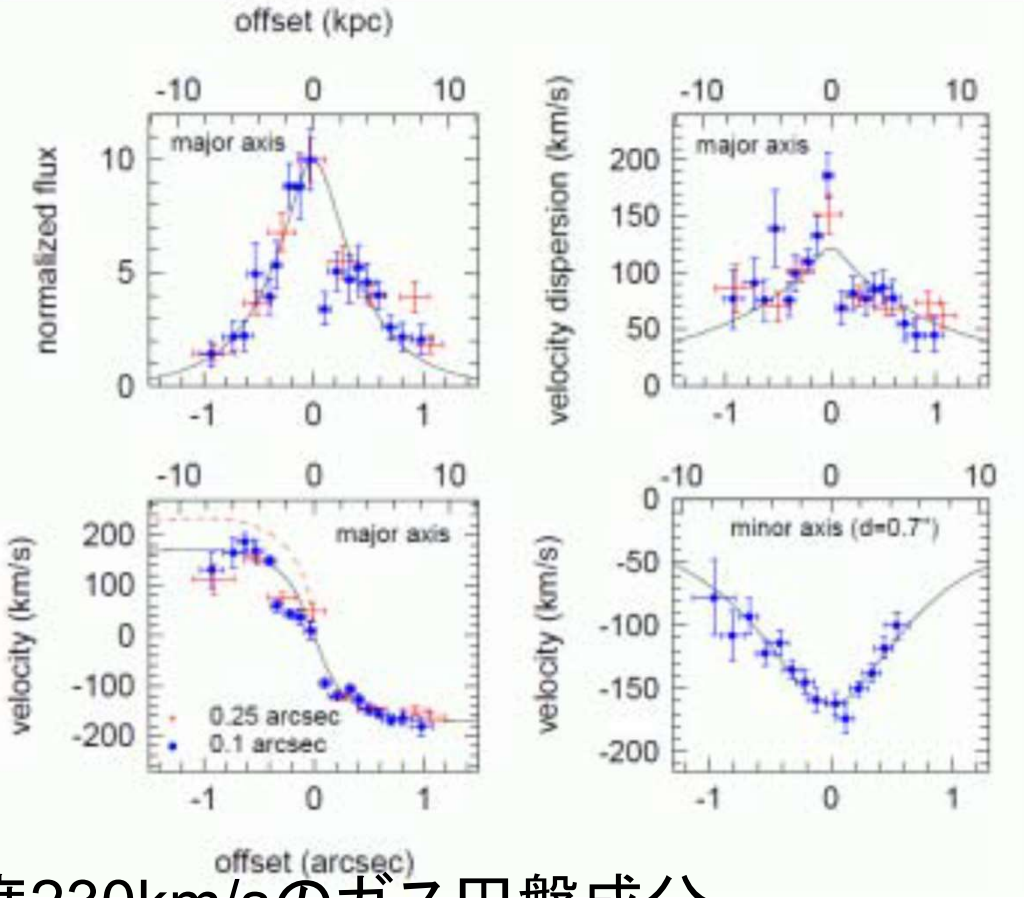

厚み～2kpc, 回転速度230km/sのガス円盤成分

⇒古い恒星円盤の形成？

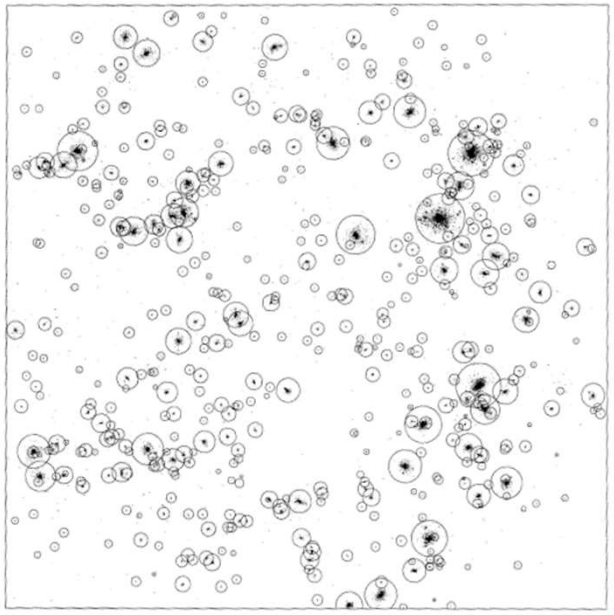

128m.n-1, 10 Mpc x 10 Mpc

スピンパラメータの確率分布

Warren et al. 1992, ApJ, 399, 405

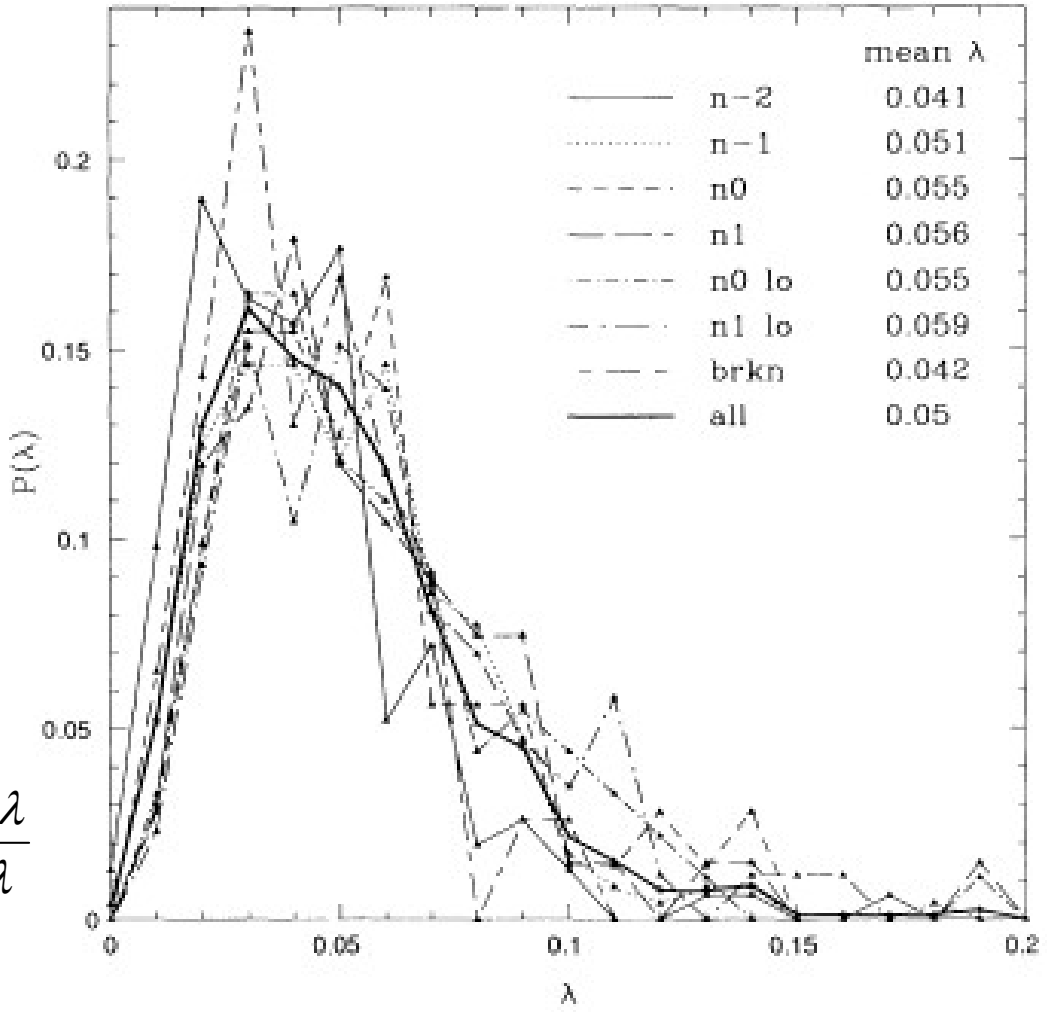

FIG. 18.—Distribution of the spin parameter (λ) for each simulations, as well as the cumulative distribution (*heavy line*). There is some dependence on the initial conditions, in that those with more power on large scales tend to have smaller spin parameters. The mean lies near 0.05, in good agreement with previous theoretical and numerical calculations.

ダークハローのスピンパラメータの確率分布

$$P(\lambda)d\lambda = \frac{1}{\sqrt{2\pi}\sigma_\lambda}\exp\left[-\frac{\ln^2\left(\lambda/\overline{\lambda}\right)}{2\sigma_\lambda^2}\right]\frac{d\lambda}{\lambda}$$

$$\overline{\lambda} = 0.05, \sigma_\lambda = 0.05$$

CDMダークマターハローの階層的合体

Navarro, Frenk, & White 1997

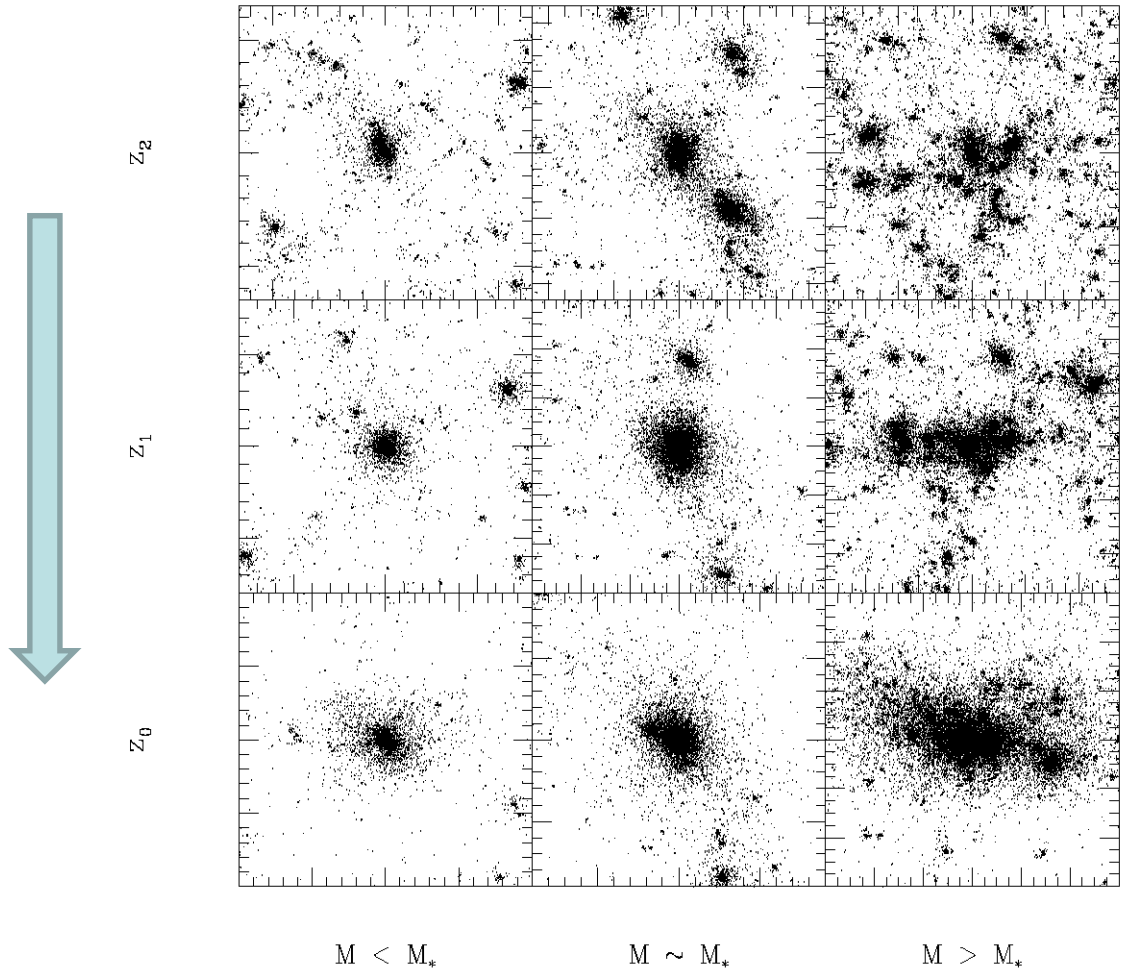

FIG. 1.—Particle plots illustrating the time evolution of halos of different mass in an $\Omega_0 = 1$, $\Lambda = 0$, and $n = -1$ cosmology. The box sizes of each column are chosen so as to include approximately the same number of particles. At $z_0 = 0$, the box size corresponds to about $6r_{200}$. Time runs from top to bottom. Each snapshot is chosen so that M_* increases by a factor of 4 between each row. Low-mass halos assemble earlier than their more massive counterparts. This is true for every cosmological scenario in our series.

CDMダークマターハローの密度分布

Navarro, Frenk, & White 1997

図： Navarro et al. 2004

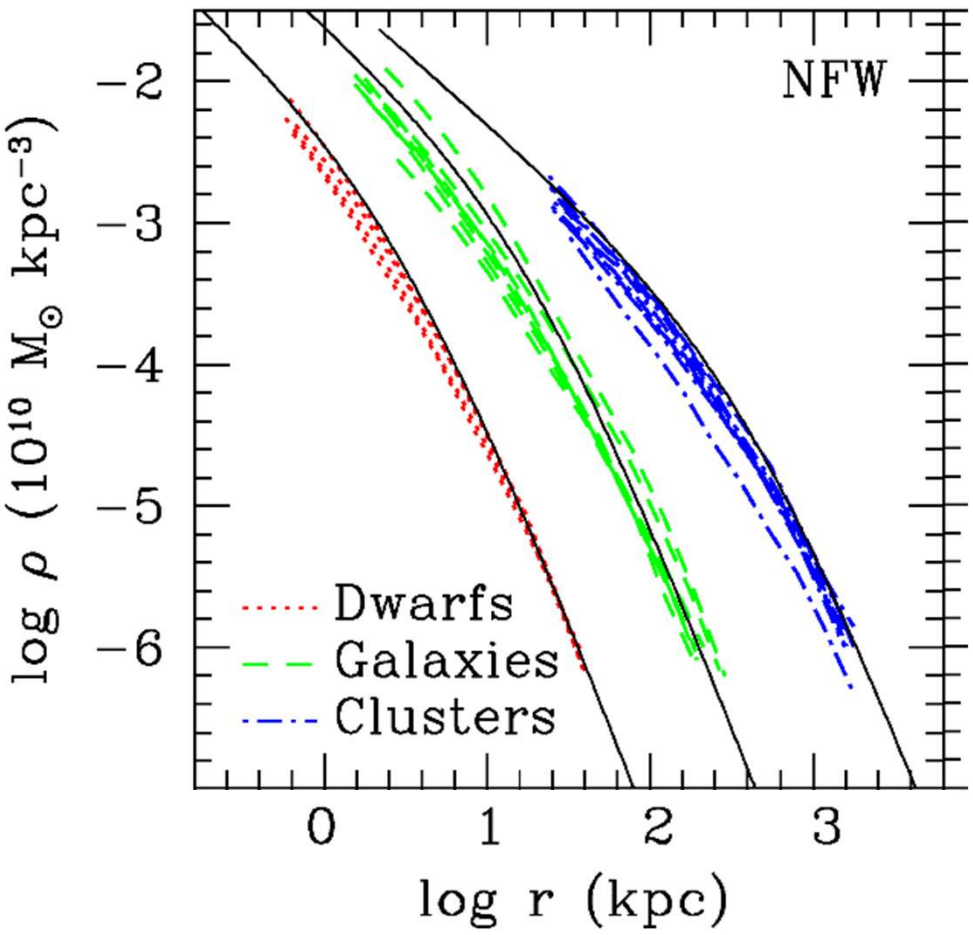

ダークハローの密度分布
（NFWプロファイル）

$$\rho = \frac{\rho_s}{\left(\frac{r}{r_s}\right)\left(1+\frac{r}{r_s}\right)^2}$$

$\rho \propto r^{-1}$ at $r \ll r_s$

$\rho \propto r^{-3}$ at $r \gg r_s$

中心でカスプ状

CDM理論での銀河形成：フィードバック

超新星フィードバック：
小さな銀河ができすぎる
のを妨げる

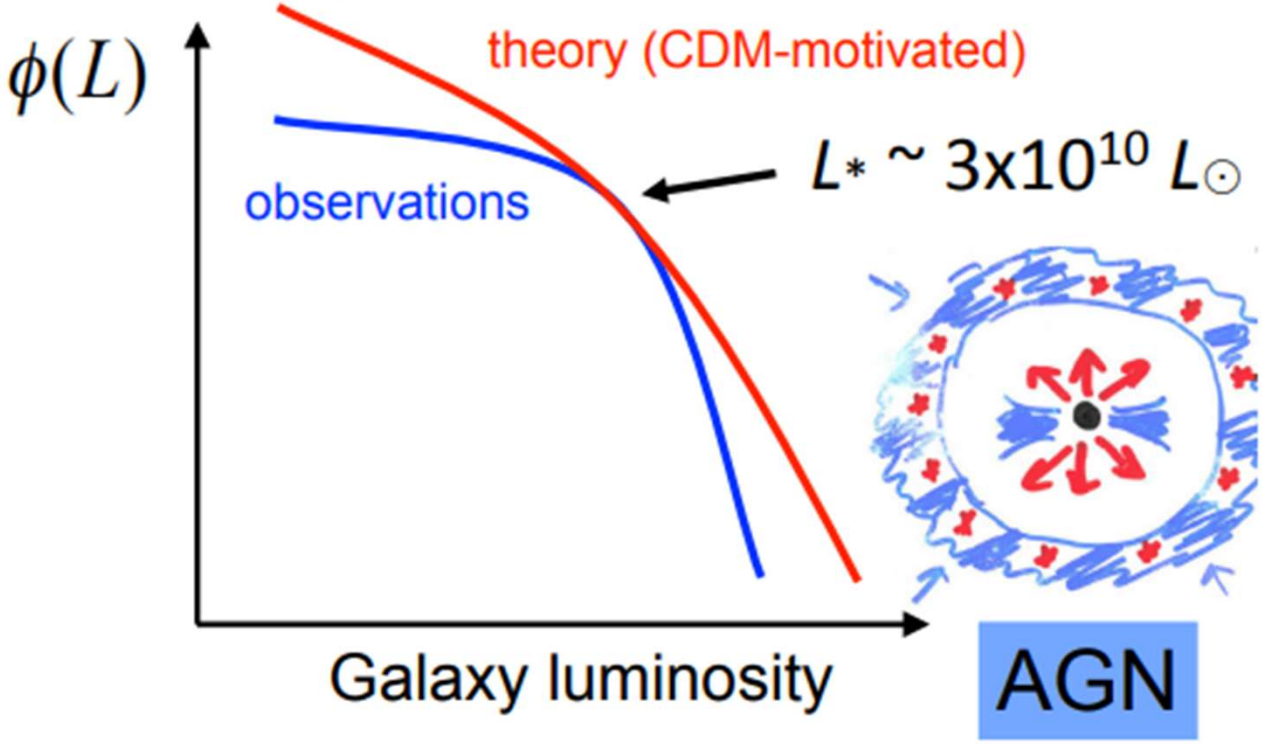

AGNフィードバック：
ガスの降着でさらに
銀河が成長するのを
妨げる

Binney & Mamon 2012

Cluster evolution as a diagnostic for Ω_0

Eke, Cole, Frenk 1996, MNRAS, 282, 263

The population of rich galaxy clusters evolves much more rapidly in a universe with critical density than in a universe with low density. Thus, counts of clusters at intermediate redshift offer the possibility of determining the cosmological density parameter, Ω_0, with a minimum of assumptions.

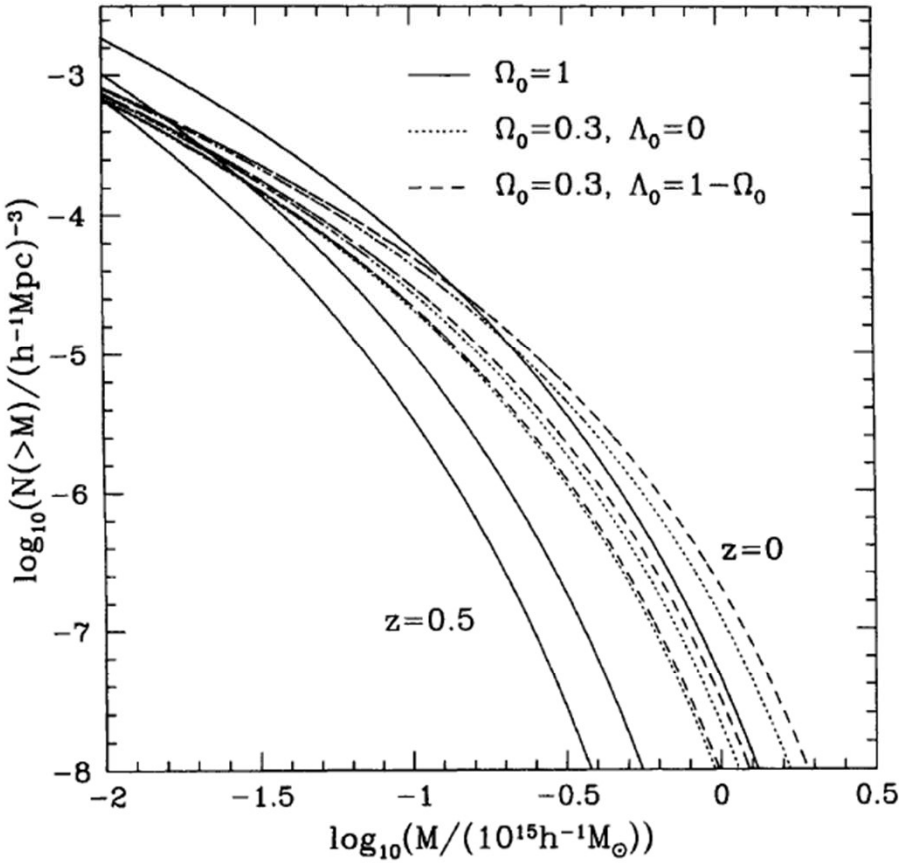

Figure 4. Predicted evolution of the cluster mass function. The comoving number density of clusters per $(h^{-1}\,\mathrm{Mpc})^3$ with masses larger than M is shown as a function of M. Solid lines correspond to $\Omega = 1$; dotted lines to an open model with $\Omega_0 = 0.3$; and the dashed lines to a flat model with $\Omega_0 = 0.3$ and $\Lambda_0 = 0.7$. Predictions for $z = 0$, $z = 0.33$ and $z = 0.5$ are plotted. There is relatively little evolution in the $\Omega_0 < 1$ cosmologies but, in an $\Omega_0 = 1$ model, the abundance of clusters declines precipitously with redshift.

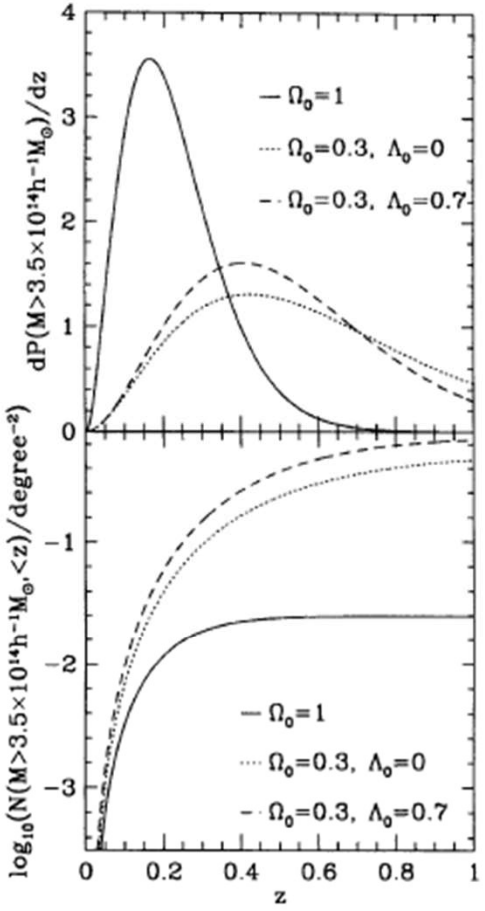

Figure 5. Upper panel: Redshift distribution of massive clusters ($M > 3.5\times10^{14}h^{-1}\,M_\odot$) in different cosmological models. The ordinate gives the probability distribution of clusters per unit redshift interval. Lower panel: Number counts of clusters with mass $M > 3.5\times10^{14}h^{-1}\,M_\odot$ out to a given redshift. The ordinate gives the count per unit area on the sky. In both panels solid lines correspond to $\Omega_0 = 1$, dotted lines to $\Omega_0 = 0.3$ and dashed lines to $\Omega_0 = 0.3, \Lambda_0 = 0.7$. The models are normalized by the value of σ_8 for which the predicted temperature function at $z = 0$ best fits the data. The low-Ω_0 cosmologies produce significantly more clusters at high redshifts than the $\Omega_0 = 1$ model.

2-color diagram

U−B

二色図

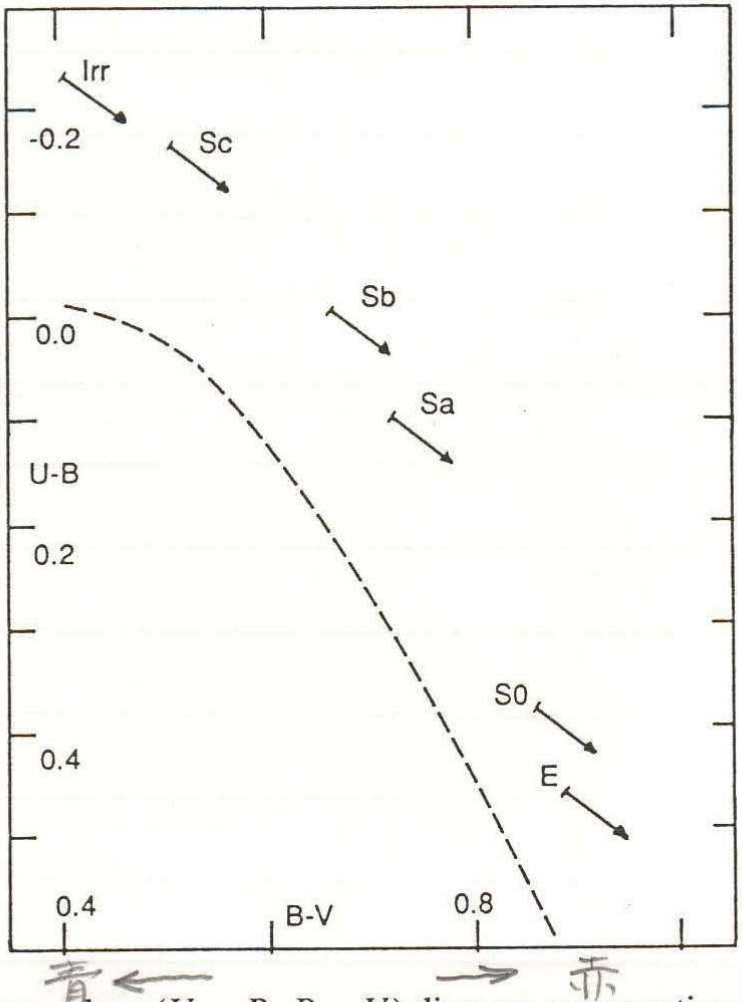

B−V

Figure 1.10 A colour–colour ($U-B$, $B-V$) diagram representing the position of normal galaxies (points) and the main sequence of stars (dashed line). The arrows indicate the effect obtained by correcting for galactic reddening, $E(B-V)=0.06$.

現在の銀河のSpectral Energy Distribution (SED)

銀河のタイプ

Sdm

Scd

Sbc

Sab

E/S0

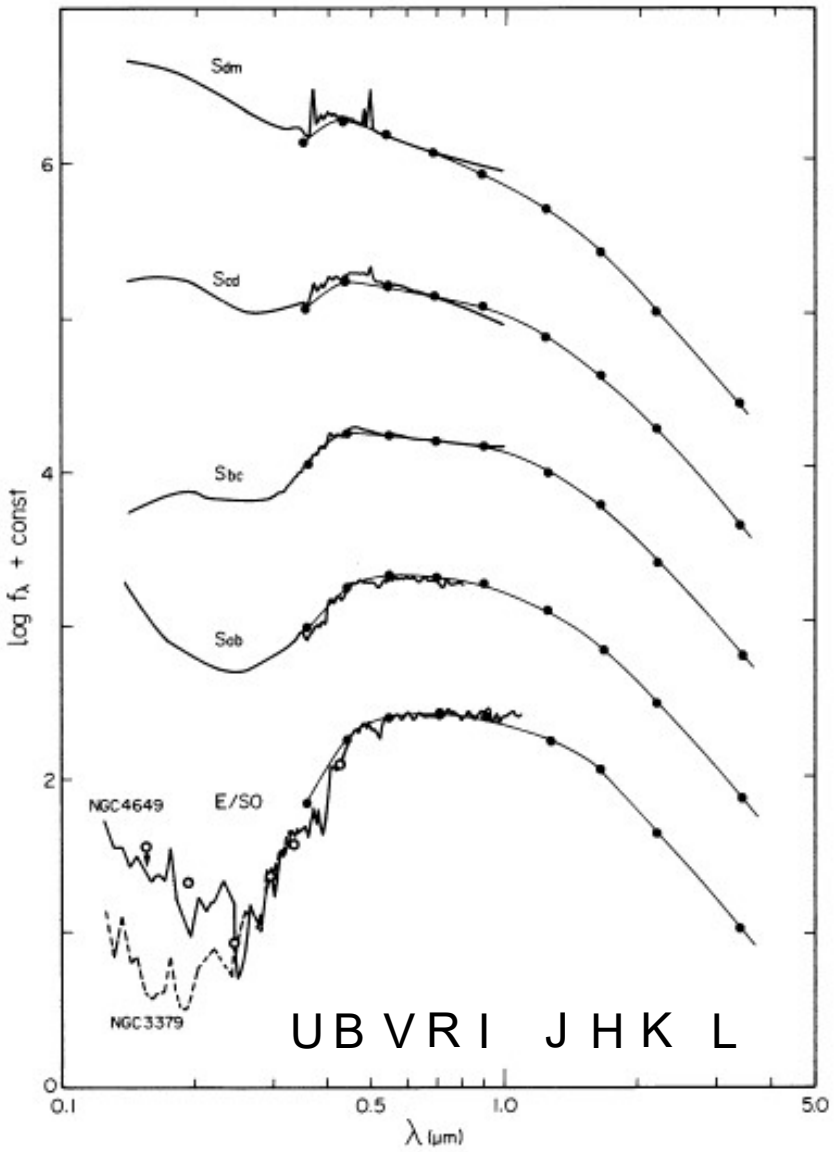

Yoshii & Takahara 1988

λ (μm)

FIG. 1.—Present-day spectral energy distribution (SED) for each galaxy type of E/S0, Sab, Sbc, Scd, and Sdm. Scale of the ordinate is arbitrary. Thick lines represent the observed SEDs. Filled circles represent the fluxes in the Johnson *UBVRIJHKL* bands synthesized by Arimoto and Yoshii (1986, 1987). Observed and synthesized SEDs are made to coincide with each other at $\lambda_R = 0.7$ μm. For the ultraviolet SED of NGC 4649, thick line corresponds to the *IUE* data and open circles to the *OAO 2* data. In the present paper we use the *IUE* SED of NGC 4649 for E/S0 galaxies. The *IUE* SED of NGC 3379 is shown only for the purpose of comparison.

B−V の時間変化：星形成時間τに対する依存性

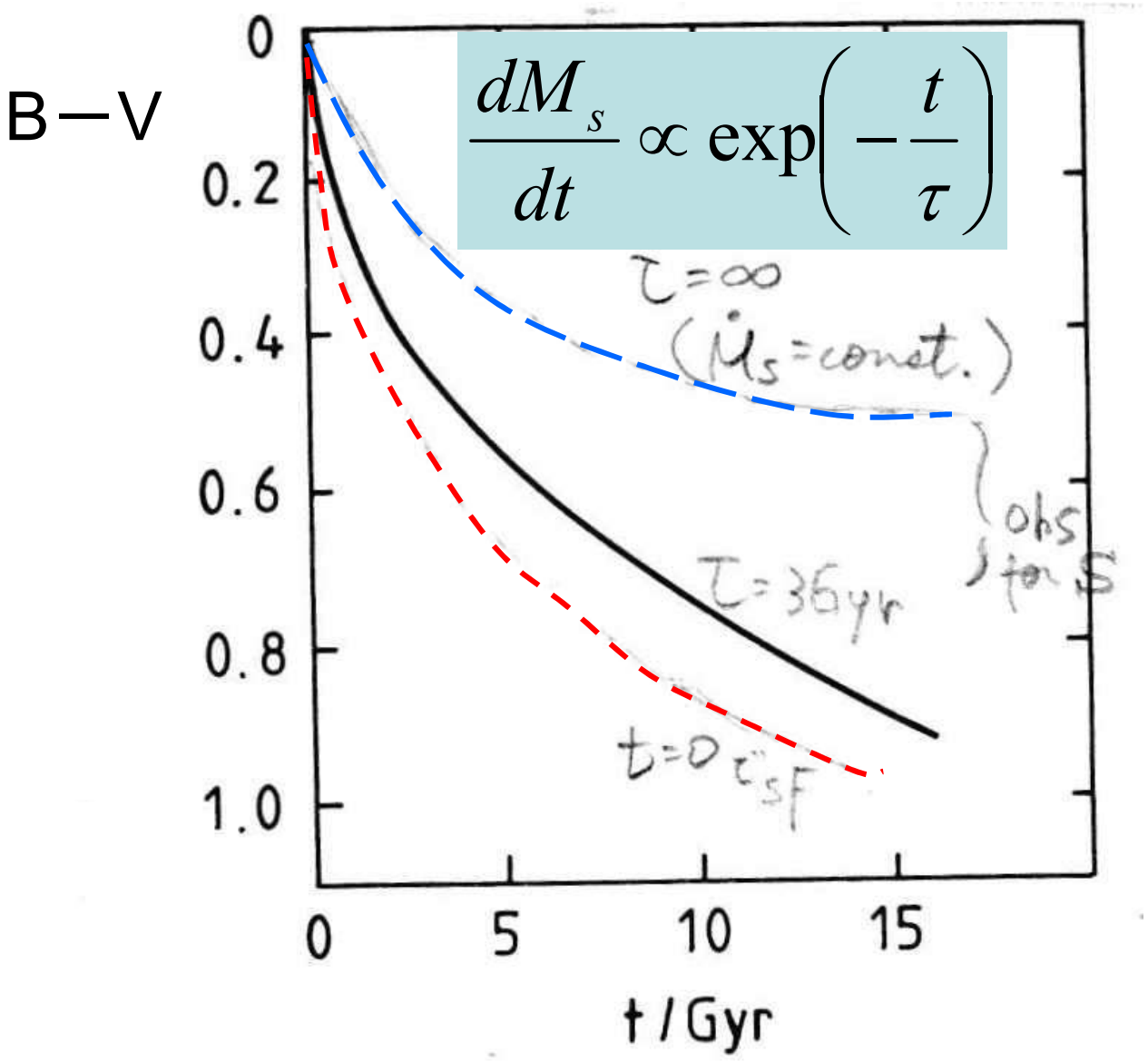

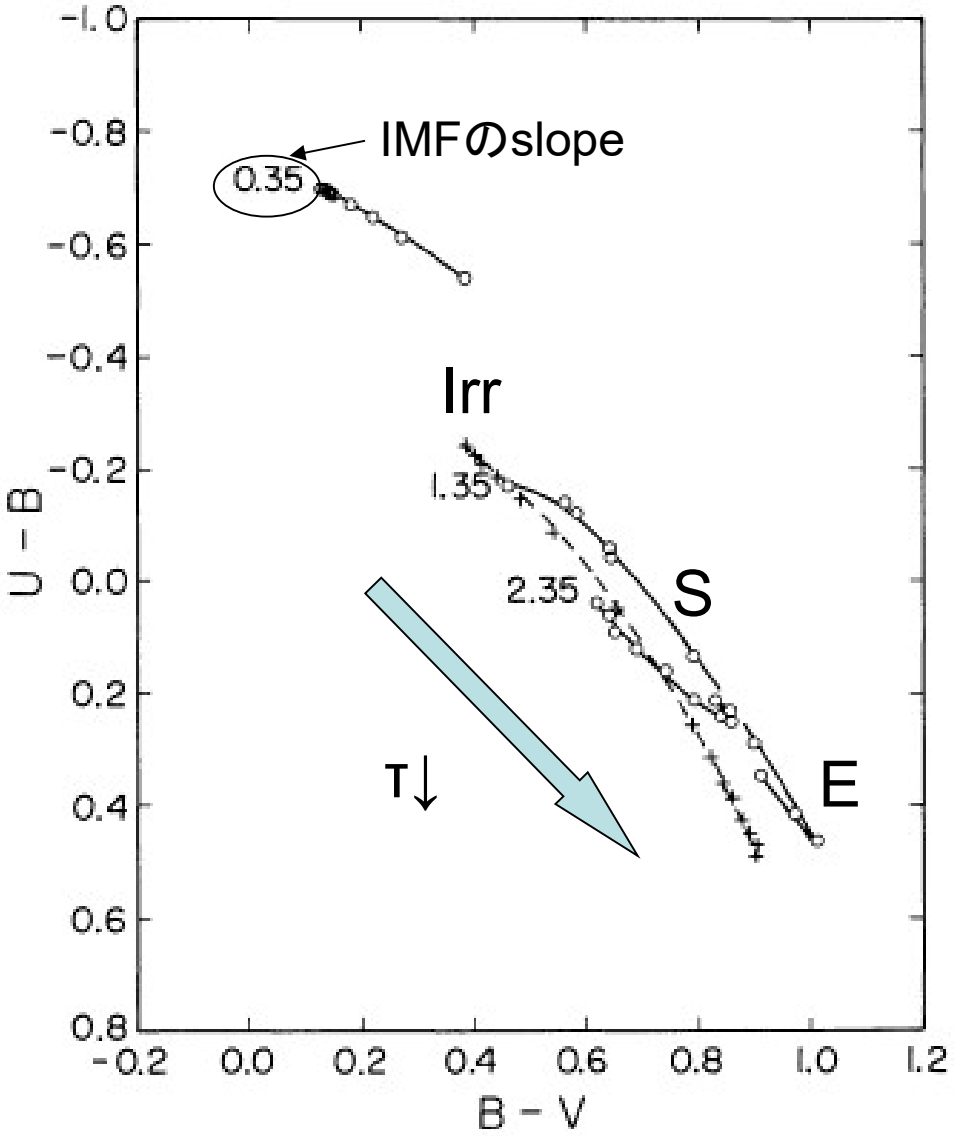

Fig. 5a. $U - B$ and $B - V$ colors of C models at 15 10^9 yr. The lines represent loci of models with varying v and constant μ. Numbers denote the adopted value of μ. Crosses denote the mean color-color relation of normal galaxies taken from de Vaucouleurs and de Vaucouleurs (1972)

様々な銀河のSEDの時間変化

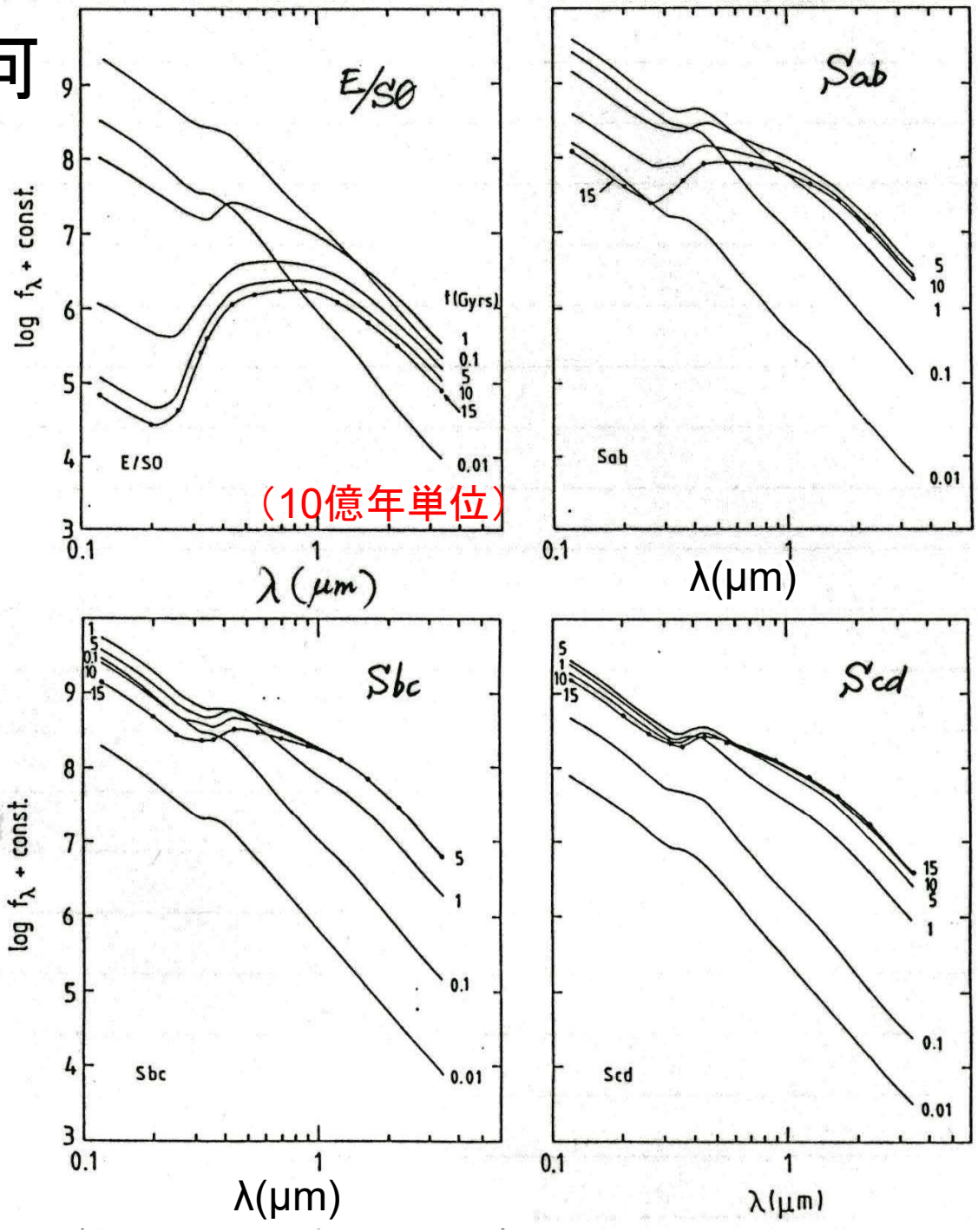

S型銀河
（円盤銀河）では、
星形成が
続いているので
短い波長域で
フラックスが
あまり減少しない。

楕円（E）銀河の標準SEDモデル

（Bruzual & Charlot 2003, MN, 344, 1000）

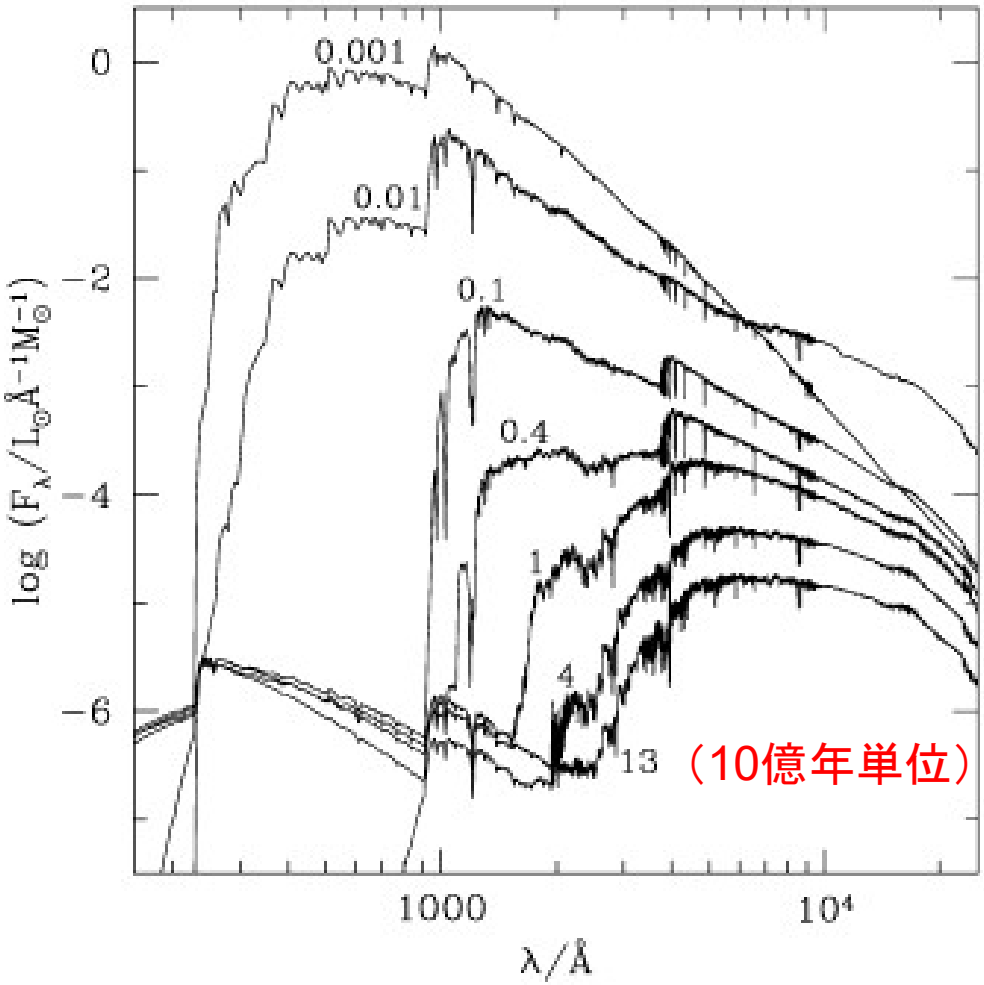

Figure 9. Spectral evolution of the standard SSP model of Section 3 for the solar metallicity. The STELIB/BaSeL 3.1 spectra have been extended blueward of 3200 Å and redward of 9500 Å using the Pickles medium-resolution library. Ages are indicated next to the spectra (in Gyr).